

EÖTVÖS LORÁND UNIVERSITY
FACULTY OF INFORMATICS
INSTITUTE OF CARTOGRAPHY AND GEOINFORMATICS

Multispectral satellite based urban greenness mapping in Budapest

Ali Dowajy

student of Cartography MSc

András Jung

Associate Professor

ELTE Institute of Cartography and Geoinformatics



Budapest, 2022

Acknowledgement

Words cannot express my gratitude to my supervisor professor András Jung for his invaluable patience and advice. I'm proud of, and grateful for, my time working with professor András. I would also like to express my deepest appreciation to all the professors in the Institute of Cartography and Geoinformatics who generously provided knowledge and expertise over two years during my study trip.

I would like to extend my sincere thanks to Eötvös Loránd University and all the employees in the institute of Cartography and Geoinformatics. Thanks should also go to the Stipendium Hungaricum scholarship, which gave me this fantastic opportunity to get a master's degree and have one of the best times of my life in one of the most beautiful cities in the world.

Finally, I must express my very profound gratitude to my mother, my father, my brothers, and my friends for providing me with unfailing support and continuous encouragement throughout my years of study. This accomplishment would not have been possible without them. Thank you.

Ali Dowajy

Table of Contents

List of Figures.....	IV
List of Tables	VI
Abstract.....	VII
1. Introduction.....	1
2. Literature review and conceptual background.....	3
2.1. Remote sensing	3
2.1.1. Data detection and output	5
2.1.2. Electromagnetic Radiation	6
2.1.3. Electromagnetic Spectrum	7
2.2. Remote sensing to detect changes in vegetation cover in urban areas	9
2.2.1. Urbanization.....	9
2.2.2. Sentinel-2	11
2.2.3. NDVI.....	11
2.2.4. Classification.....	12
3. Methodology	14
3.1. Study Area:	14
3.2. Acquisition of Satellite Data and Preprocessing.....	16
3.3. Preprocessing	19
3.3.1. Atmospheric correction.....	19
3.3.2. Cloud removal.....	19
3.4. Processing.....	23
3.4.1. NDVI.....	23
3.4.2. Classification.....	24

3.4.3. Accuracy assessment.....	25
3.4.4. Land change detection	27
4. Results and Discussion.....	28
4.1. NDVI.....	28
4.2. Classification.....	37
4.3. Accuracy assessment	40
4.4. Land change detection	43
5. Conclusion	48
References	49
ANNEX	59

List of Figures

Figure 1. Remote sensing process. Source: (Subramaniam & Mallast, 2017).	4
Figure 2. Energy interaction in the atmosphere and at the Earth's surface. Source: (Tempfli et al., 2009)	5
Figure 3. Electromagnetic wave components. Source: (Chuvieco & Huete, 2009).	6
Figure 4. Electromagnetic Spectrum. Source: (Chuvieco & Huete, 2009).....	7
Figure 5. Healthy plants absorb a lot of visible light while reflecting a lot of near-infrared light (left). Vegetation that is unhealthy or sparse absorbs more visible light and reflects less near-infrared light (right). Source: (Simmon, 2022).....	11
Figure 6. Methodology flowchart followed.	14
Figure 7. Budapest location. A: Location of Hungary.....	15
Figure 8. An example of an image that cannot be used for processing.	17
Figure 9. Cloud removal flowchart followed.....	21
Figure 10. The image that used to fill in the gaps for the month of June.	22
Figure 11. A part of Budapest before and after the clouds were removed for the image on 28/05/2017.	23
Figure 12. Comparison of NDVI image representation when using different values for Built-up area.....	28
Figure 13. NDVI images for Budapest (1/3).	29
Figure 14. NDVI images for Budapest (2/3).	30
Figure 15. NDVI images for Budapest (3/3).	31
Figure 16. Line chart of NDVI values for Margit Sziget.....	32
Figure 17. Line chart of NDVI values for Népliget.....	32
Figure 18. Line chart of NDVI values for Városliget.....	33
Figure 19. Variation of vegetation cover between April 2020 and 2021.....	33
Figure 20. 3D model of NDVI values for Margit Sziget.	34
Figure 21. 3D model of NDVI values for Népliget.	35
Figure 22. 3D model of NDVI values for Városliget.	36
Figure 23. Classified images based on NDVI images for Budapest. (1/3).....	38
Figure 24. Classified images based on NDVI images for Budapest. (2/3).....	39

Figure 25. Classified images based on NDVI images for Budapest. (3/3).....	40
Figure 26. Line chart of the Kappa index and Overall accuracy.	42
Figure 27. Line chart of land change.	44
Figure 28. Budapest land change in July between each year and the following year.....	45
Figure 29. Budapest land change between 2017 to 2021 June.	46
Figure 30. Vegetation changes of Budapest districts.....	47

List of Tables

Table 1. Regions of EMR used for remote sensing and their principal applications.....	8
Table 2. The datasets and bands specifications used in this research.	16
Table 3. Images of the missing months.	16
Table 4. Datasets used from Sentinel-2 satellite.	18
Table 5. The images that contain the clouds, and the target images.....	22
Table 6. NDVI reclassified image classes.	24
Table 7. Interpretation of Kappa index.	26
Table 8. Ground control points.	27
Table 9. Classes of the reclassified NDVI images.....	37
Table 10. Kappa index and overall accuracy.	41
Table 11. Confusion Matrix for April 2021.....	42
Table 12. Land change proportion.	43
Table 13. Changes in the top three districts in Budapest.....	47
Table 14. Changes in the top three districts that have become greener in Budapest.....	47

Abstract

The importance of urban green space has over the years grown into an indispensable component in urban planning and design, as vegetation plays an irreplaceable role in urban ecosystem services. Therefore, monitoring and studying the distribution of biomass for urban vegetation is necessary because of its impact on the life and health of urban residents. Remote sensing technology has provided many advantages for studying and monitoring urban vegetation cover, due to its temporal and spatial characteristics in overcoming the scarcity of information, and the short revisit period, which helps to make quick, more effective and impactful decisions. The normalized difference vegetation index (NDVI) was calculated for the city of Budapest in order to study and assess the behavior of vegetation cover there, based on the Sentinel-2 imagery spanning over five years between the years 2017 and 2021. Vegetation change has been extensively studied in the three most green urban areas. The results showed that 2021 was the least green year in general, and this corresponds to the average rainfall and temperature in that year. Also, NDVI threshold-based supervised classification was performed to determine land cover changes, as the city of Budapest has become greener during these years by about 100 hectares.

Keywords: Budapest, Urbanization, Urban vegetation, Remote sensing, NDVI, Sentinel-2, Vegetation cover monitoring

1. Introduction

Urbanization is experiencing rapid growth all over the world, as it is reducing the presence of urban vegetation cover, and disrupting the urban ecosystem, which is helping to stimulate the phenomenon of climate change, and creating the urban heat island (UHI), which refers to the difference in temperature between areas inside and outside the city (Bartholy et al., 2020).

Urban vegetation has become a major element in urban planning for cities for urban sustainability, because of its various effects on the health of citizens and their well-being of living, as it contributes significantly to facing the effects of urban and climate change by decreasing temperature, air pollution, and noise, etc (Jabbar et al., 2021).

Given the important role played by urban vegetation cover in serving the local climate of the city and the ecosystem, urban green areas must be carefully studied and monitored, as the availability of a correct estimate of the biomass of urban vegetation is the main step in facing the problems of urbanization and its impact on the climate, in order to provide decision-makers and city planners with this information in order to be taken into account and relied on in the planning of cities for the future (Jim, 2013).

The methods used in estimating and mapping urban vegetation cover have developed and become more accurate, as field measurements were adopted in the past, but it consumes a very long time and a relatively large number of skilled crews, in addition, it is stressful work (Li et al., 2020). As for now, remote sensing is widely used, as it is considered a great tool for estimating and mapping the biomass of urban green spaces due to its temporal and spatial characteristics, short revisit period, and wide coverage, more efficiently and on a larger scale than the traditional method (S. Liang & Wang, 2020).

Furthermore, remote sensing technology has proven to be great in observing and understanding the impact of urban vegetation on the environmental problems of cities (Jung et al., 2018).

The city of Budapest, located in Hungary, was chosen in order to study the vegetation cover and its changes, as Budapest has a continental climate, with relatively high summer temperatures and frequent heat waves being a problem (Páldy et al., 2005). Sentinel-2 images with a resolution of 10 meters were used from 2017 to 2021 from April to September of each year, to calculate

NDVI indicator, in order to study the vegetation cover of the city of Budapest and study the change of urban vegetation cover in the three urban greenest areas in it in order to judge Budapest and see the behavior of the urban vegetation cover in it if it becomes greener or grayer, and seeing how suitable and healthy it is to live by studying the behavior of urban vegetation and providing results and data on which future studies can be conducted.

2. Literature review and conceptual background

It is essential to review background information, concepts, and related studies in order to analyze land cover changes. This chapter focuses on remote sensing, urbanization, NDVI, and the Sentinel 2 program, as well as a review of relevant literature.

2.1. Remote sensing

Remote Sensing (RS) can be defined as the process of obtaining, interpreting, and processing images and information about an object through analysis of the data obtained by the sensor without being in physical contact with it (Schultz & Engman, 2000). This can be done by using recording or real-time sensor devices mounted on aircraft, spacecraft, satellites, etc. Detecting and differentiating objects on the Earth's surface entails detecting and recording the radiant energy reflected or emitted by objects or materials on the surface.

This technique consists of various components. Figure 3 shows, energy source, is a condition for implementing a remote sensing process, which determines whether the remote sensing process is passive, where the sun is the source of electromagnetic energy and the sensors measure the reflection of solar radiation at visible, near-infrared, and mid-infrared wavelengths (Dong & Chen, 2017). Active sensors provide their own energy source for lighting. The sensor emits radiation directed at the target to be examined. The radiation reflected from this target is detected and measured by the sensor.

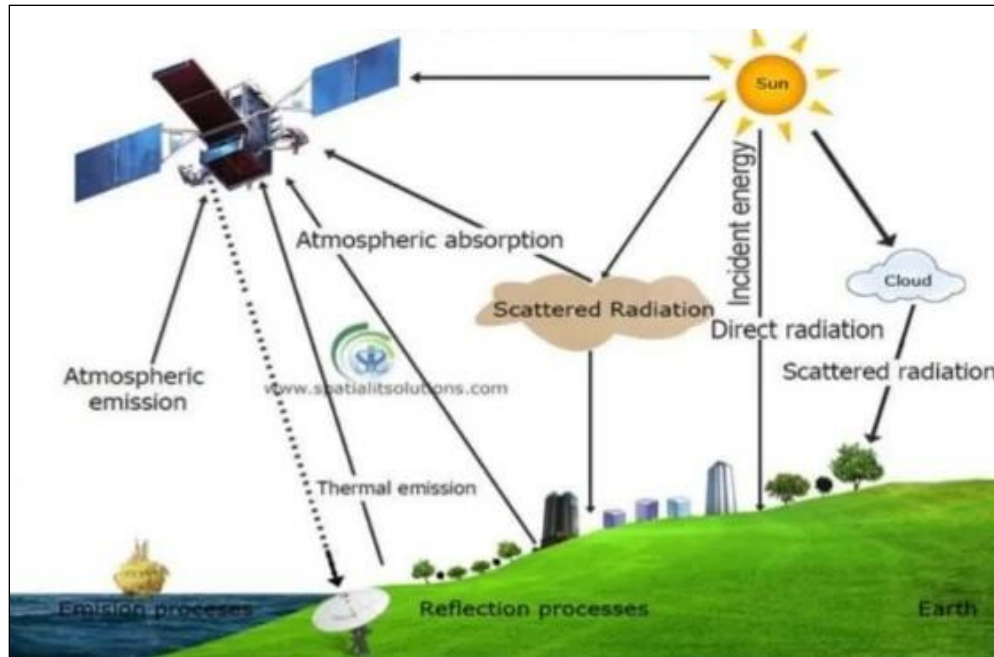


Figure 1. Remote sensing process. Source: (Subramaniam & Mallast, 2017).

When solar radiation incident on the Earth's surface, Figure 2, the incident radiation can be:

- ❖ Transmission is the process by which incident radiation passes through matter.
- ❖ Reflection is the process through which incoming radiation bounces off the surface of a material in a particular, predictable direction. The angle of incidence and reflection are always equal and opposing (Schultz & Engman, 2000).
- ❖ Scattering is when incoming radiation is distributed or spread out unpredictably in numerous directions, including the direction from whence it came.
- ❖ Absorption is the process by which incoming radiation is absorbed and then subsequently released.

Radiation is emitted by objects based on their temperature and emissivity (Singh & Reddy, 2018). The remotely sensed data contains both spatial and spectral information (size, shape, and orientation), (tone, color, and spectral signature).

While traveling from the source to Earth features and from Earth features to the sensor, the electromagnetic radiation interacts with the atmosphere. The electromagnetic radiation changes its characteristics during this path due to energy loss and wavelength shifts, which impacts the sensor's ability to detect the Electromagnetic radiation. This interaction often leads to atmospheric noise.

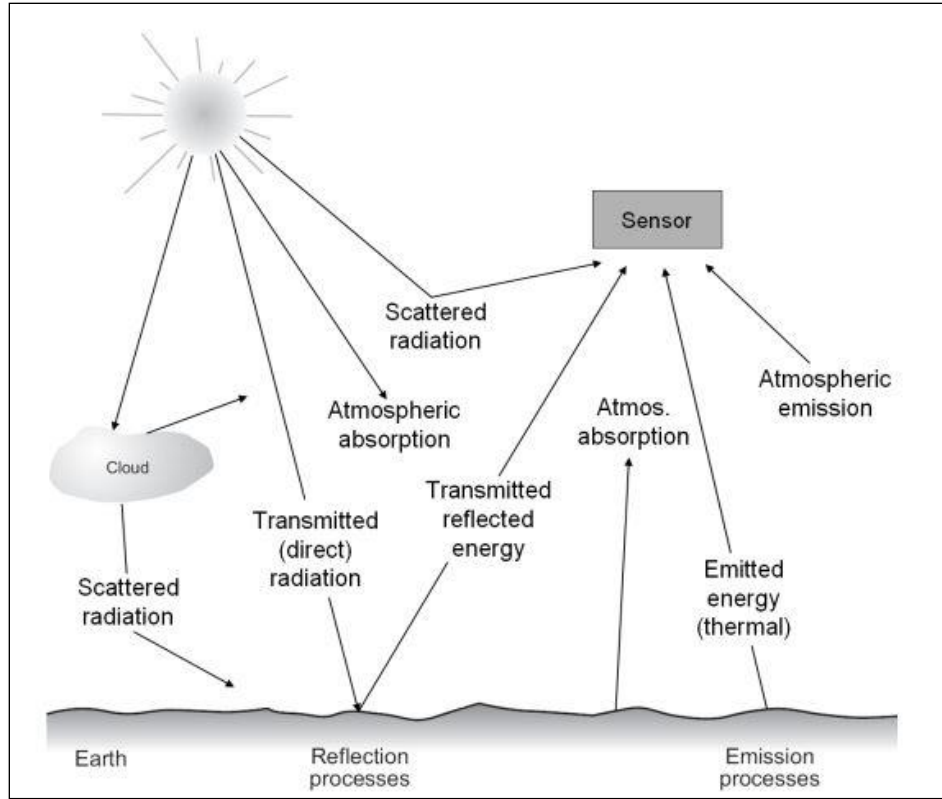


Figure 2. Energy interaction in the atmosphere and at the Earth's surface. Source: (Tempfli et al., 2009)

2.1.1. Data detection and output

The sensor, which records the variation of radiant energy reflected or emitted by objects or surface material, is the most significant component in remote sensing.

Different regions of the electromagnetic spectrum are responsive to different types of sensors. The recording system's job is to convert the energy sensed by the sensor into a form that can be understood. This is accomplished by dividing the incoming energy into different wavelength bands using beam splitters and filters, then converting the energy in each wavelength band into an electrical signal. The electrical signal is processed to give radiometric data for each band, which is recorded in digital format (Chuvieco & Huete, 2009).

2.1.2. Electromagnetic Radiation

Electromagnetic radiation (EMR) is one of the universe's most basic kinds of energy. Electromagnetic energy includes visible light, radio waves, ultraviolet rays, radiant heat, X-rays, etc. All of this energy is fundamentally similar and propagates according to fundamental wave theory (Chuvienco & Huete, 2009). As shown in Figure 3.

Electromagnetic radiation is a dynamic kind of energy that travels at the speed of light ($c = 3 * 10^8 \text{ m} * \text{sec}^{-1}$) as a wave motion. This fundamental wave theory depicts electromagnetic energy as moving at the speed of light in a harmonic sinusoidal pattern.

$$c = v\lambda \quad (1)$$

where v represents frequency, λ represents wavelength, and c represents velocity. Although wave theory can readily describe many aspects of electromagnetic energy, particle theory can shed light on how electromagnetic energy interacts with matter. It is suggested that electromagnetic radiation is made up of a number of discrete units called photons/quanta. Quantum energy is:

$$Q = h(c/\lambda) \quad (2)$$

where Q is the energy of quantum, h is plank's constant.

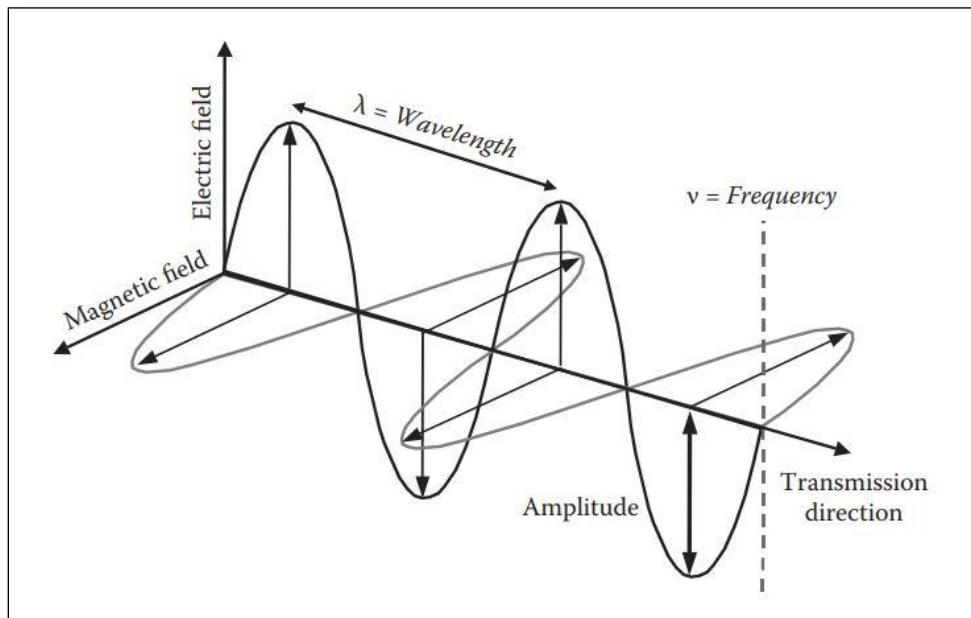


Figure 3. Electromagnetic wave components. Source: (Chuvienco & Huete, 2009).

2.1.3. Electromagnetic Spectrum

Most common remote sensing devices work in one or more of the electromagnetic spectrum's visible, infrared, and microwave bands.

The transmission of energy from the surface in different portions of the electromagnetic (EM) spectrum is measured by most sensors to record information about the Earth's surface, Figure 4. Because the Earth's surface varies in nature, the transmitted energy changes as well, allowing for the creation of images of the surface. This energy variation is apparent to human eyes in the visible portion of the electromagnetic spectrum. Sensors detect energy fluctuations in both visible and non-visible spectrum regions (Singh & Reddy, 2018).

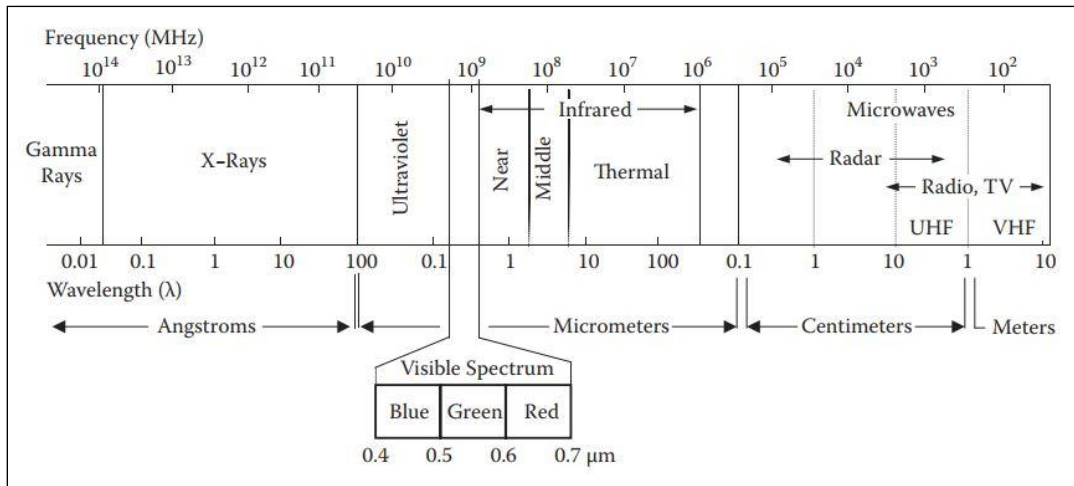


Figure 4. Electromagnetic Spectrum. Source: (Chuvieco & Huete, 2009).

The interaction of electromagnetic radiation with the material on the earth's surface, which is reflected, scattered, or emitted from the material, provides the basis for remote sensing. The interaction of electromagnetic radiation with the earth's surface characteristics generates reflected and/or emitted signals known as spectral signatures (Singh & Reddy, 2018). Detection, identification, and analysis of earth's surface material rely heavily on spectral response patterns. Table 1, presents the spectral regions of the visible wavelengths down to the thermal infrared.

Table 1. Regions of EMR used for remote sensing and their principal applications.

Spectral regions	Wavelength (μm)	Principal application
Visible Region	0.4 – 0.7	The visible spectral region where it can be detected by the eye.
Blue	0.45 – 0.52	Water penetration, land use, vegetation characteristics, sediment
Green	0.52 – 0.60	Green reflectance of healthy vegetation
Red	0.63 – 0.69	Vegetation discrimination because of red chlorophyll absorption
Reflected Infrared	0.7 – 3	Reflected infrared region where it exceeds the sensitivity range of the eye.
Near infrared	0.76 – 0.90	Vegetation vigor, biomass, delineation of water features, land forms/geomorphic studies
Mid infrared	1.55 – 1.75	Vegetation moisture content, soil moisture content, snow and cloud differentiation
Mid infrared	2.08 – 2.35	Differentiation of geological materials and soils
Thermal Infrared	3 – 14	Thermal infrared is used in urban climate and environmental studies, mainly for analyzing land surface temperature (LST) patterns.
Thermal IR	3.0 – 5.0	For hot targets, viz., fires and volcanoes
Thermal IR	10.4 – 12.5	Thermal sensing, vegetation discrimination, volcanic studies

Source: (Singh & Reddy, 2018)

2.2. Remote sensing to detect changes in vegetation cover in urban areas

2.2.1. Urbanization

Urbanization has contributed to bringing about significant changes in the urban vegetation cover in terms of quality and quantity (Tan et al., 2013), and in most cases, the main responsible for the decrease and deterioration of urban vegetation cover is the urban expansion. It is expected that by 2050, urban areas will be home to approximately 66% of the world's population (Uçar et al., 2020).

The provision of diverse ecosystem services by public urban green spaces, defined as vegetated places within cities that are open to the general public (municipal parks, public playgrounds), is a significant component of the urban quality of life (Gren et al., 2013). Public urban green spaces reduce the urban heat island effect (Gábor & Jombach, 2010), and offer space for inhabitants to engage in recreational and cultural activities including sports, nature viewing, and social interaction (Dickinson & Hobbs, 2017).

Recent research suggests that adequate access to nearby public green places is good for people's well-being and mental health, and urban nature is viewed as resilient infrastructure in times of disaster, such as the COVID-19 pandemic (Venter et al., 2020). As a result, it's important to give people and city planners the information they need on the location and quality of public urban green areas (Kabisch et al., 2016), so that may be taken into account in future planning.

Nonetheless, most cities lack comprehensive and open data sets on public urban green areas, which are an essential requirement for such studies (Feltynowski et al., 2018). There has been a growing interest in urban vegetation mapping recently, as it affects the local climate of the city, including temperature and humidity. This interest in studying urban vegetation is due to the response to global climate change, which is a major problem for cities (Kraas & Mertins, 2014). The growing number of urban residents, traffic congestion, and the persistent urban heat island effect are all factors that directly affect global climate change (Pongracz et al., 2016).

In order to address such urban problems and their impacts on climate change, urban vegetation plays an important role in service to the ecosystem (Pickett et al., 2011). The availability of accurate spatial distribution data of urban vegetation is the main step in addressing urban problems.

Researchers are becoming increasingly aware of the importance of urban vegetation as their understanding of ecosystem services grows, as the study of urban vegetation is critical to achieving sustainable urbanization goals (El-mezouar et al., 2011). In recent years, remote sensing technology has provided several advantages for urban vegetation studying and mapping, for more accurate assessments of ecosystem processes. Relying on remote sensing technology in urban planning provides quick, more effective, and impactful decisions (Jung, 2007).

Urban remote sensing due to the temporal and spatial characteristics can help overcome the paucity of reliable and repeatable information on urban vegetation (Churkina et al., 2010).

The correct estimation of urban plant biomass provides important information about the current environmental state of cities, which is used in many fields to conduct planning, management, and Preservation of urban vegetation, tree biomass can be estimated using field measurements (Gibbs et al., 2007), GIS and remote sensing methods (Lu, 2006).

Traditional method biomass estimation includes measuring structural features for individual tree species and calculating biomass using allometric equations (Sousa et al., 2015). However, this process is costly, wasteful of resources, and labor-intensive. A number of methods have been proposed for urban vegetation mapping using different methods such as random forest classification (Puissant et al., 2014), fuzzy rule-based classification (Hecht et al., 2008), or convolutional neural networks (Wegner et al., 2016).

During the last three decades, low and medium-resolution satellite photos, such as MODIS and Landsat images, have been used to detect and monitor urban land changes across wide regions. However, because of the low spatial resolution of these pictures, they are only useful for detecting large-scale urban land expansion and not for capturing urban land changes at precise scales (Qian et al., 2015). Vegetation can be well detected using multi-spectral optical imagery (Hu et al., 2016). Very high-resolution LIDAR data (Hancock et al., 2017), or imagery captured by Unmanned Aerial Vehicles (UAV) (Suab & Avtar, 2020), are the best data sources for mapping and detecting vegetation cover, but due to the difficulty and cost of obtaining this type of data, remote sensing techniques might be utilized to map and estimate such urban green biomass more efficiently at a greater scale than the traditional method, where images with high to medium precision are used, such as Landsat, or synthetic aperture radar (SAR) imagery, and in particular Sentinel-2.

2.2.2. Sentinel-2

Sentinel-2 is an Earth observation mission from the Copernicus Program (European Commission and European Space Agency) that acquires high spatial resolution images. The mission consists of two satellites operating in the same sun-synchronous (180°) orbit, Sentinel-2A and Sentinel-2B, launched on 23 June 2015 and 7 March 2017, respectively. The swath width is 290 km, with a repeat cycle of five days under the same viewing conditions. A MSI is installed on both satellites. The MSI measures the Earth's reflected radiance in 13 spectral bands, with four bands at 10 m, six bands at 20 m, and three bands at 60 m of spatial resolution. (ESA, 2022).

2.2.3. NDVI

On a remote sensing image, there are numerous indices for highlighting vegetation-bearing areas. The NDVI is a frequently used and well-known index. It's an important vegetation index, widely used in studies of worldwide environmental and climatic change (Brumbaugh, 1996), and it is used to determine if the target being observed includes living green vegetation or not, using remote sensing measurements.

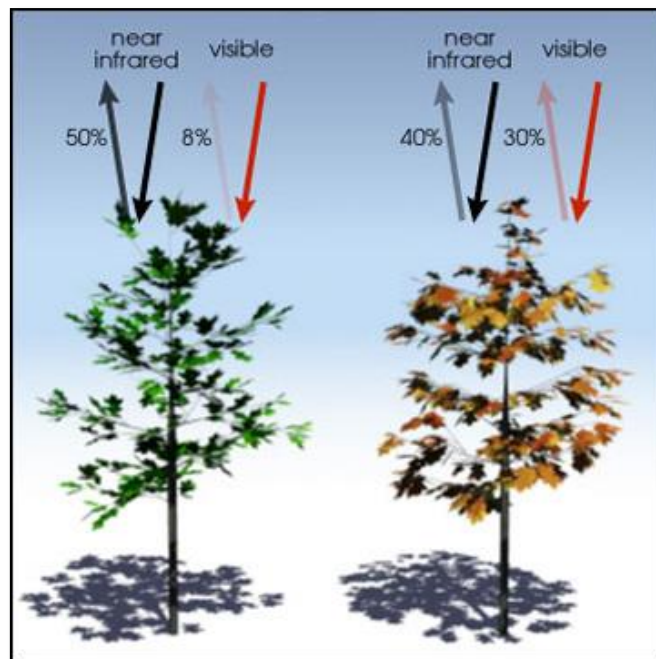


Figure 5. Healthy plants absorb a lot of visible light while reflecting a lot of near-infrared light (left). Vegetation that is unhealthy or sparse absorbs more visible light and reflects less near-infrared light (right). Source: (Simmon, 2022).

It has been relied on NDVI to study changes in urban vegetation cover, and it has been proven that the NDVI indicator accurately detects various changes in land cover (Zaitunah et al., 2018). This research aims to analyze the vegetation cover areas and their changes in Budapest. The NDVI index is a powerful tool for understanding past vegetation, monitoring it in the present, and predicting its future (Xing et al., 2020).

2.2.4. Classification

Landsat-8, Sentinel-2A/2B products, Moderate Resolution Imaging Spectroradiometer (MODIS), LiDAR, UAV images, contributed significantly to the land cover classification. Within the framework of NDVI, the various land cover classification methods are divided into two categories: index-based classification and machine learning-based classification.

2.2.4.1. Index-Based Classification

In index-based classification, each pixel in the image is classified using a threshold of NDVI value. (Ehsan & Kazem, 2013), employed an NDVI value to detect changes in Landsat images. (Montandon & Small, 2008), used an NDVI threshold for land cover classification and change detection in several places. For epidemiological investigations in Spain, (Gascon et al., 2016) employed the NDVI value as a marker of plant surroundings. (da Silva et al., 2020), for example, used NDVI indices, to classify the land cover in Brazil.

Classification is performed in machine learning-based methods using two approaches: unsupervised and supervised approach. In the unsupervised approach, this technique does not use prior information about the study area, that is, it does not include the training phase, rather, the use of algorithms is selected to group a remotely sensed data set with similar spectral characteristics into specific clusters (Mohd Hasmadi et al., 2009). The second stage is to identify the land cover that represents each group of image units with similar spectral characteristics.

In the supervised approach, supervised classification is based on the premise that a user can select sample pixels in an image that are indicative of specific classes, and then direct the image processing software to utilize these training sites as references for classifying the rest of the pixels in the image, The study site's ground cover is known, thus training locations are chosen based on

that knowledge. The number of categories to which the image is to be classified is determined by the user (Oseni et al., 2020).

2.2.4.2. methods based on machine learning

The methods based on machine learning can be divided into two parts:

1. Traditional methods based on machine learning:

The traditional methods based on machine learning depend on popular algorithms, such as k-nearest neighborhood (KNN) (Laaksonen & Oja, 1996), Support Vector Machine (SVM) (Kecman, 2005), Random Forest (RF) (BREIMAN, 2001), etc. (Daryaei et al., 2020), utilized the RF algorithm to accurately detect vegetation on UAV and Sentinel-2A images. (Liu et al., 2018), employed Sentinel-1A, DEM, Landsat-8, and Sentinel-2A images were used to determine the type of forest using the RF algorithm.

(Zhang et al., 2017), evaluated different bands of Sentinel-2A images and compare the index-based classification with the SVM algorithm to classify the different regions in these images into four classes. (Appiah Mensah et al., 2019), four different types of remote sensing images (Landsat-4, Landsat-7, Sentinel-2A, and Worldview-3) were applied and classified using machine learning algorithm to detect the change in Ghana. While the methods based on deep learning use the developed deep learning models.

(Timilsina et al., 2020), used CNNs for urban tree cover changes in Australia using the LiDAR data. (P. Liang et al., 2018), also used Stacked Denoising Auto Encoder (SDAE) to classify remote sensing images, which showed that SDAE outperforms SVM and ANN. (Luo et al., 2020), proposed a hybrid convolution neural network (H-ConvNet) to improve the performance of urban land cover mapping using Sentinel-2A images.

At the end of this study, using 10-meter-resolution Sentinel 2 multiple times data, the NDVI index was calculated to study vegetation changes, and the NDVI-based supervised classification was performed to classify vegetation cover in order to determine land change.

3. Methodology

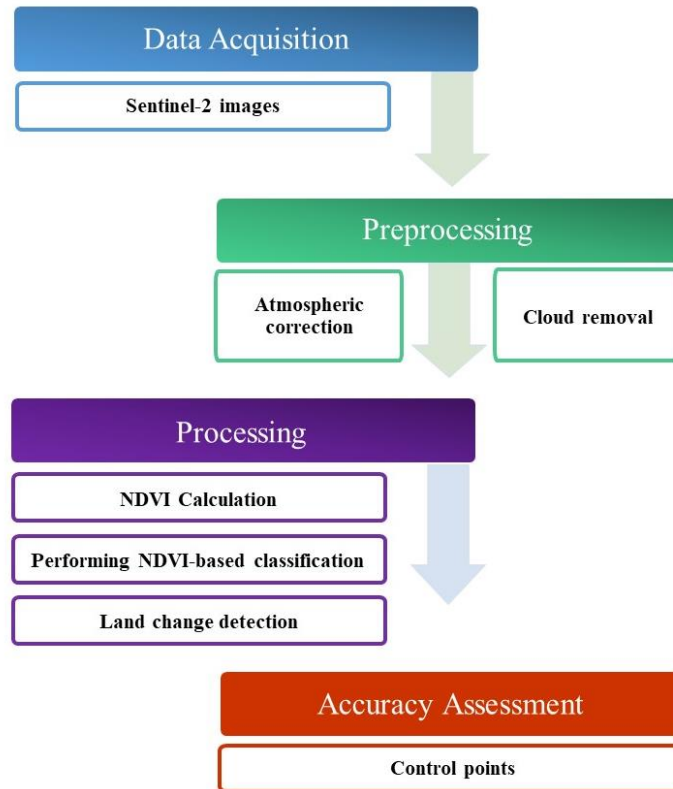


Figure 6. Methodology flowchart followed.

There were four stages to the project. The first stage was a literature review for the use of remote sensing techniques in the study of urban vegetation maps. Then, in order to proceed with satellite image acquisition, the study area was chosen. Geographic information system software, QGIS® 3.22.4 (Białowieża), was used to process the images. Finally, the results were gathered, analyzed and presented. The methods utilized in the project are described in full below.

3.1. Study Area:

Budapest was selected for this study. The study period is 5 years from 2017 to 2021, from April to December each year.

Study area general description:

The study area is Budapest, see Figure 7, the capital of Hungary, it is located in the north-central part of Hungary, it is one of the most economically important cities in Eastern Europe, and it serves

as Hungary's undisputed political, administrative, and cultural hub. Located along the Danube River, which crosses the city in a north-south direction, and divides it into western (Buda) and eastern (Pest) parts (Péter, 2021). According to the Hungarian National Statistical Office, the total population is 1.7 million people living in 525 square kilometers, which means more than, 3200 people per square kilometer average population density. This number varies greatly between the districts of the city. Also, the general built-up area is 52 percent, which could increase with time.

The city is divided into 23 districts (Buzási, 2022), which differ slightly in terms of land use and vegetation cover but differ radically in urban areas. It should be noted that the Buda side (the Danube's right side) has far more green areas than the Pest side. In Pest, urbanization has increased and flourished greatly due to the nature of the flat terrain suitable for urbanization, unlike Buda, for which there is a delay in urbanization due to rather a complex terrain and mountains, but from another point of view, mountains and hills covered with forests contribute greatly to relieving the summer heat and maintaining fresh air.

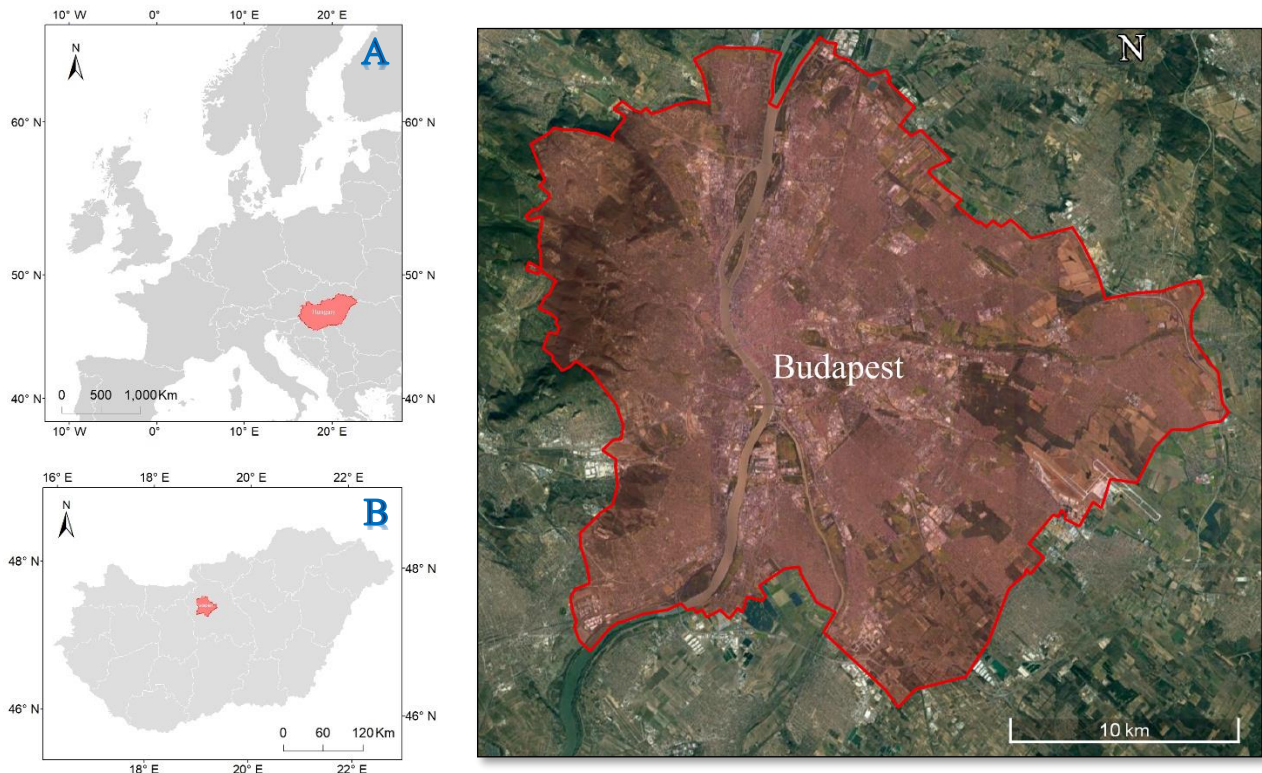


Figure 7. Budapest location. A: Location of Hungary. B: Location of Budapest in Hungary. Source: Created by the author.

3.2. Acquisition of Satellite Data and Preprocessing

For this research, Sentinel-2 images were used due to the open-access facility, high resolution, and temporal availability. The datasets were downloaded from the website European Space Agency (Copernicus) (<https://scihub.copernicus.eu/>), which is the European Union's Earth Observation Program, looking at our planet and its environment for the benefit of Europe's citizens. The specifications of Sentinel-2 bands used in this study are presented in Table 2 (ESA, 2020a).

Table 2. The datasets and bands specifications used in this research.

Satellite	Band	Resolution	Central wavelength (nm)	Wavelength (nm)
Sentinel 2	B02 - Blue	10 m	492.4	458 - 523
	B03 - Green	10 m	559.8	543 - 578
	B04 - Red	10 m	664.6	650 - 680
	B04 - NIR	10 m	832.8	785 - 899

Images were downloaded for all months from April to September from 2017 to 2021, except for some months, where the cloud coverage did not provide any acceptable visibility of Budapest Table 3.

Table 3. Images of the missing months.

Year	Month
2017	April
2018	May
	June
2019	May
2020	June

Figure 8. is an example of satellite images that cannot be used for processing.



Figure 8. An example of an image that cannot be used for processing.

The best available Sentinel-2 images were downloaded at Level 2A, except two images were downloaded at Level 1C, see Table 4. Where level 1C is a pre-processed product providing Top-Of-Atmosphere (TOA) reflectance with geometric corrections. The level 2A Bottom-Of-Atmosphere (BOA) reflectance is obtained by processing the product from Level 1C, to remove any intervening atmospheric effects from the Sentinel images (ESA, 2020b).

Table 4. Datasets used from Sentinel-2 satellite.

Year	Month	Day	
		Level 2A	Level 1C
2017	May	28	
	June	14	
	July		29
	August		11
	September	05	
2018	April	28	
	July	14	
	August	08	
	September	30	
2019	April	20	
	June	27	
	July	17	
	August	21	
	September	22	
2020	April	24	
	May	22	
	July	28	
	August	25	
	September	14	
2021	April	24	
	May	09	
	June	16	
	July	08	
	August	10	
	September	06	

3.3. Preprocessing

3.3.1. Atmospheric correction

The Dark Object Subtraction (DOS) method was used for atmospheric correction of Sentinel-2 Level 1C images, using the QGIS® plugin SCP (Semiautomatic Classification Plugin). Dark object subtraction (DOS) is an image-based technique based on the premise that certain pixels in the image are in complete shadow and that their radiances received on the satellite are due to atmospheric scattering (path radiation). This assumption is coupled with the fact that very few targets on Earth's surface are completely black, so an assumed minimum reflectance of one percent is better than zero percent (Chavez, 1996).

DOS looks for the darkest pixel value in each band. Any number larger than zero must be due to atmospheric scattering, assuming dark objects do not reflect light. By removing this value from each pixel in the band, the scattering is erased. This simple technique works well for haze correction in multispectral data, but it is not suitable for hyperspectral data (Jadhav & Singh, 2018).

There is another way to apply the correction in addition to that, the software is Sen2cor, which is provided by the European Space Agency (ESA). “It performs the atmospheric, terrain, and cirrus correction of TOA Level 1C input data, to achieve BOA Level 2A product” (ESA, 2020c).

3.3.2. Cloud removal

Cloud removal is a major pre-processing step for remote sensing because it has significant negative effects on data processing for many remote sensing applications such as classification, change detection, etc., as it obscures and prevents obtaining a clear view from the Earth's surface for the majority of all-optical sensors, so, it is critical to be able to reconstruct the information of the cloud-contaminated Earth (Ozkan et al., 2018).

Traditional cloud removal can be divided into three classes (Shen et al., 2015) which are, respectively, spatial-based methods, spectral-based methods, and multi-temporal based methods.

Spectral-based methods use the bands with intact information as a reference to reconstruct the bands' missing information, by establishing the link between bands (Shen et al., 2015).

By creating polynomial models between bands, some spectral-based methods overcome this challenge. The results of spectral-based methods offer a good visual effect and accuracy in general, but they can't handle situations where all bands are missing information.

For all bands, spatial methods can handle missing information. They presume that the missing information and the rest of the information have the same statistical law and geometric structure, allowing the missing information to be reconstructed from the rest of the information. Missing information can be reconstructed for all bands using spatial-based algorithms, although they can only handle missing areas of small sizes (J. Zhang et al., 2015).

Multi-temporal-based methods reconstruct missing information using homogeneous data from other times as a reference. It outperforms the above two methods in the reconstructing of large missing information. (Lorenzi et al., 2013).

Because satellites can revisit the same area at different periods, the multi-temporal data acquired provides complementary information. This may be used to reconstruct densely clouded areas (Y. Zhang et al., 2019).

In the remote sensing image sequences, the temporal-based methods presume that the ground objects' category and geometric positions seldom change during short time periods (Gao & Gu, 2017).

Recently, some deep learning-based multi-temporal cloud removal methods have been proposed. For example, (Sarukkai et al., 2020) introduced the deep neural network in the multi-temporal cloud removal mission. For a small number of images, it is possible to discard the clouds manually for instance (Wilson & Sader, 2002).

Based on the available data, available tools, and the number of images, a manual method was used to remove the clouds, see Figure 9, which depends on replacing the clouds' areas with another cloudless image.

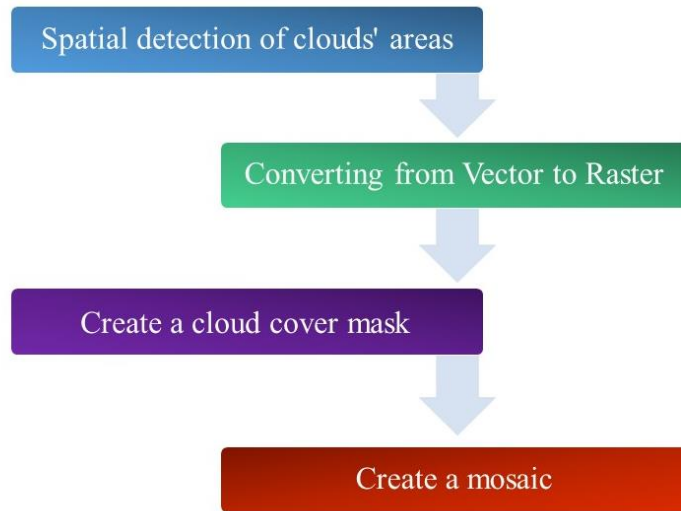


Figure 9. Cloud removal flowchart followed.

The working methodology of the used method is as follows:

1. Spatial detection of clouds' areas.

A Shapefile file was created and digitized for the clouds' spatial areas.

2. Converting the clouds' areas from Vector to Raster.

Converting the Shapefile to a raster image, where it becomes possible to create a mask for the areas of the cloud.

3. Create a cloud cover mask.

When the mask was created, a problem was faced due to an error in the SCP (Semiautomatic Classification Plugin), where the areas of the clouds have no data values, and they are supposed to be 0. So, Fill no data instruction from QGIS was used to replace the No data values with 0.

4. Create a mosaic.

After that, mosaics were made, and cloudless images were obtained.

Target images from a period of time were used as close as possible to the reference image, and in the absence of this, target images 2021 were used for the same month. Table 5 shows the images that contain the clouds, and the target images to fill where the clouds are.

Table 5. The images that contain the clouds, and the target images.

Reference Image			Target image		
Year	Month	Day	Year	Month	Day
2017	May	28	2020	May	22
2017	June	14	2017	June	24
2017	September	5	2021	September	6
2018	July	14	2021	July	8
2021	April	24	2020	April	24

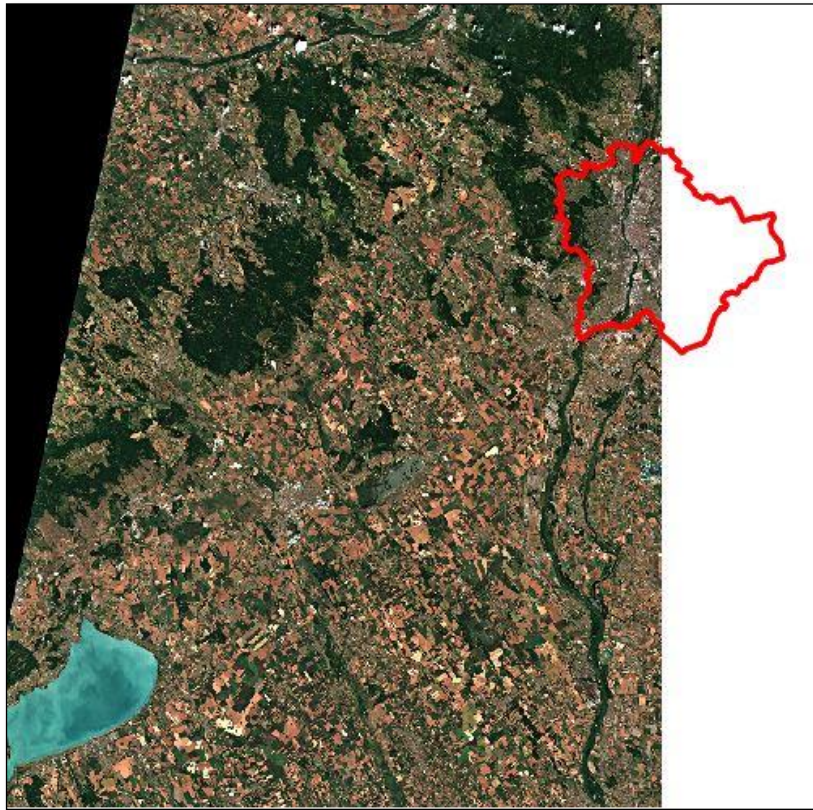


Figure 10. The image that used to fill in the gaps for the month of June.

On the 6th of June 2017, the target image does not cover the entirety of Budapest, but it covers the place of clouds, so it was used Figure 10.

The clouds were removed from the images shown in Table 5. Figure 11, shows a part of Budapest before and after the clouds were removed for the image on 05/28/2017.

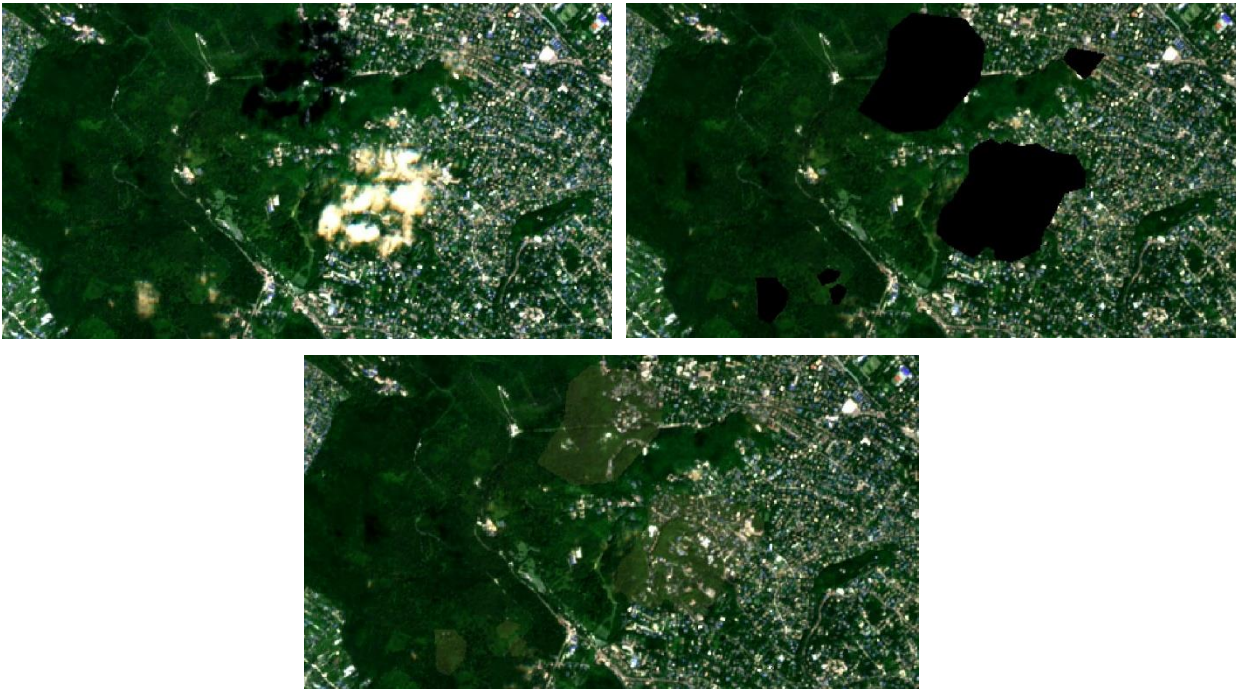


Figure 11. A part of Budapest before and after the clouds were removed for the image on 28/05/2017.

3.4. Processing

The raster files of the bands obtained from the previous step were used to calculate Normalized Difference Vegetation Index (NDVI). All the calculations were processed in the geographic information system software QGIS® 3.22.4 (Białowieża).

3.4.1. NDVI

The NDVI is one of the most often used indicators of vegetation, it provides pixel-level information on the existence of vegetation, as well as the quantity and quality of vegetation (Orhan et al., 2014). The NDVI index range is between -1 and +1, a higher NDVI index value means a higher concentration of vegetation on the ground (Al Shaikh, 2015). In general, a negative NDVI index value denotes non-green areas such as barren, river, sea, and built-up areas, whereas a positive value denotes green areas (Abdullah et al., 2019).

In addition, the NDVI value may also be used to determine the health of plants. Because it is expected that healthy plants will have higher NDVI levels than unhealthy plants (Phan et al., 2020).

Because vegetation reflects strongly in the near-infrared bands and absorbs strongly in the red bands, NDVI is calculated using the reflection of vegetation in both the near-infrared and red bands of an image (Mahajan & Bundel, 2016). NDVI was calculated using the Equation 3, proposed by Kriegler (1969) (Huang et al., 2021).

$$NDVI = \frac{NIR - RED}{NIR + RED} \quad (3)$$

Where NIR [Band 8] and RED [Band 4] represent the near-infrared and the red band of Sentinel-2A image product, respectively with a resolution of 10 m.

In this study, NDVI images were calculated for all months to be studied (April to December) for all years (2017 to 2021) in order to create a time series of vegetation change over time. After calculating the NDVI images, the images were clipped relative to the Budapest boundary.

3.4.2. Classification

Before performing a classification, the NDVI image has been reclassified into five classes in Table 6 in order to perform the NDVI image-based classification.

Table 6. NDVI reclassified image classes.

Class	Number
Water	1
Built-up area	2
Grass	3
Shrub	4
Forest	5

The images were classified by Orfeo ToolBox (OTB) using the supervised classification method and the algorithm Shark Random Forest (Shark RF). This was done with the help of the reclassified NDVI image.

Shark Random Forest:

Random Forest is a supervised machine learning technique that is made up of many decision trees (Tempa & Aryal, 2022). For each pixel, Random Forest's algorithm generates a number of decision trees, after that, each of these trees decides the class that the pixel should be classified to, and then the classification class is chosen for the pixel that gets the largest amount of choices from the trees (Belgiu & Drăgu, 2016).

Shark Random Forest's algorithm is effective and accurate compared to other classification methods, Shark Random Forest's algorithm is superior to Random Forest's algorithm in the ability to benefit from the prediction capabilities of the Shark implementation (Boret & Cesaro, 2019).

Different training samples were selected for each image, but in general, the number of training samples ranged from 65 to 85 by the digitization of specific polygons. Each training field was assigned a number from 1 to 5 representing land cover classes include forest, shrub, grass, urban and built-up areas (residential, industrial, transportation, and, roads), and water (rivers, lakes).

The spectral signature defined in the training set is used to classify land cover. Each class is determined by what is similar in the training set, according to the digital image classification software, the NDVI images are classified into several classes based on the NDVI value (Taufik et al., 2019).

Orfeo Tool Box (OTB)

OTB is an open-source project for processing remotely sensed imagery, developed in France by CNES (www.orfeo-toolbox.org, accessed 10 March 2021). It is an image analysis toolkit that is openly available and controllable by other open-source software packages and command-line tools. The algorithms implemented in OTB were applied in this work through the QGIS software. The algorithms implemented in OTB were applied in this work through the QGIS® 3.22.4 (Białowieża) software.

3.4.3. Accuracy assessment

To evaluate the accuracy of classified image maps, they should be compared to reference data that is presumed to be correct (Foody, 2002).

A confusion matrix was used to assess the accuracy of classification, as well as overall accuracy. The classification is not complete until the accuracy of the classification is evaluated using the well-known Kappa statistics (Forkuor & Cofie, 2011).

Overall accuracy

This accuracy generates the overall results of the confusion matrix, it is obtained by dividing the total number of correctly classified pixels (diagonal values) by the total number of pixels (Tewabe & Fentahun, 2020).

Kappa coefficient

The Kappa Coefficient measures how well classification and truth values agree, This statistic is particularly useful for determining the accuracy of predictive models by comparing the predictive model's agreement with a collection of manually measured sample points (J.J.Wynne & Jenness, 2005). The Kappa index was used to determine the proportion of well-ranked pixels to the total number of pixels examined (Congalton, 1991).

Each kappa statistic value was assessed by adopting Landis and Koch standards (Landis & Koch, 1977). Evaluation Criteria Table 7.

Table 7. Interpretation of Kappa index.

Kappa statistic	Strength of Agreement
0.00 - 0.20	Slight agreement
0.21 - 0.40	Fair agreement
0.41 - 0.60	Moderate agreement
0.61 - 0.80	Substantial agreement
0.81 - 1.00	Almost perfect agreement

In this study, 100 ground control points were used to validate the classified images by measuring the points manually from Google Earth. Table 8 shows the number of ground control points measured for each class.

Table 8. Ground control points.

Number of points	Class
15	Water
28	Built-up area
19	Grass
19	Shrub
19	Forest

3.4.4. Land change detection

Land cover and land change are major climatic factors, and remote sensing data studies are sometimes the only method to determine these differences (Arévalo et al., 2020), as change detection can be used to determine and evaluate changes in a variety of surface phenomena over time (Jusoff & Senthavy, 2003).

The point of determining the change of vegetation cover is to discover each class of vegetation cover to which class it will change (Tewabe & Fentahun, 2020).

Arithmetic differences for the image, Land Cover Classification Comparisons, change vector analysis, principal component analysis, and the differencing of (NDVI) are among the most commonly used land change detection methods (H. Zhang et al., 2009).

In this study, a classification comparison of vegetation cover was used. For each period, the areas covered by each land cover class were compared. The GDAL Sieve function was used on the land change images to remove small isolated pixels, which removes raster polygons that are smaller than a given threshold size in pixels, and replaces them with the pixel value of the largest neighbor (Warmerdam et al., 2022).

4. Results and Discussion

4.1. NDVI

For the NDVI values categories, it was relied on matching the NDVI images with satellite images and matching each class with the corresponding reality to represent the reality as much as possible. Depending on the reference categories of NDVI values (Ya'Acob et al., 2014), values less than 0 mean that it is water, but as in Figure 12, there are errors in the categories when adopting that, so these values were adopted for the land cover classes.

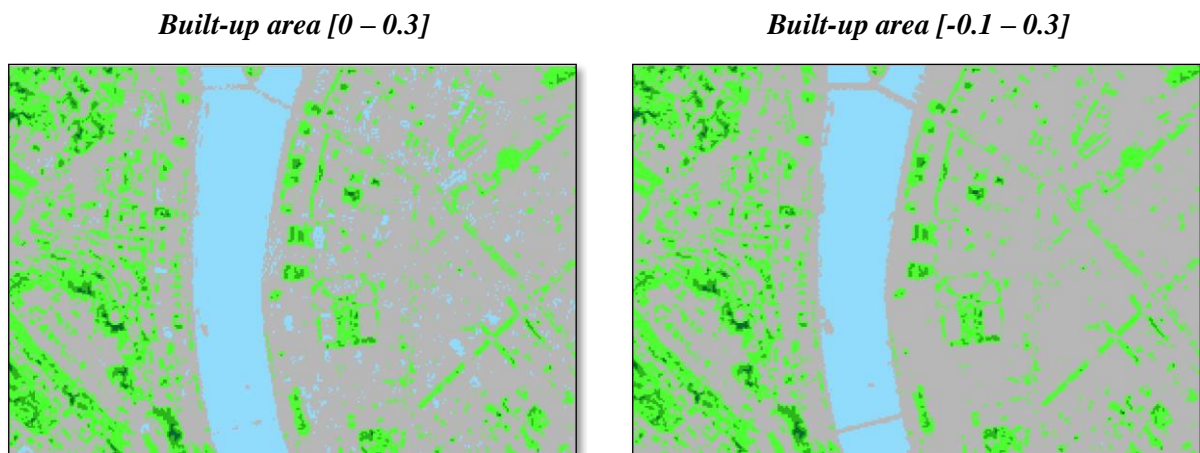
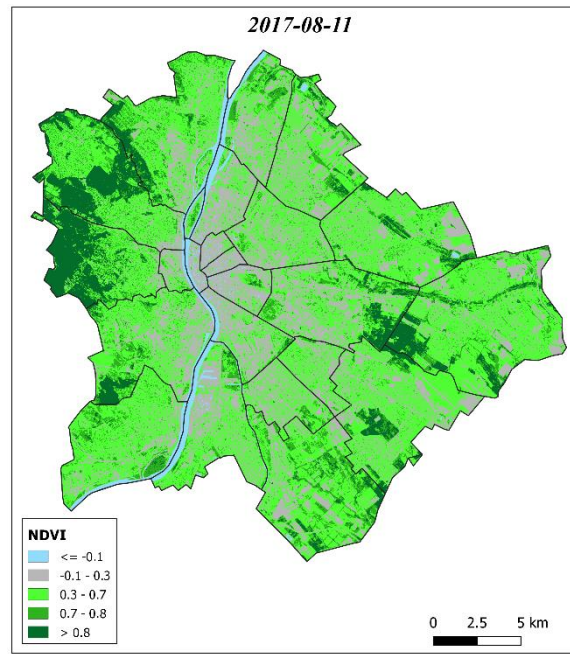
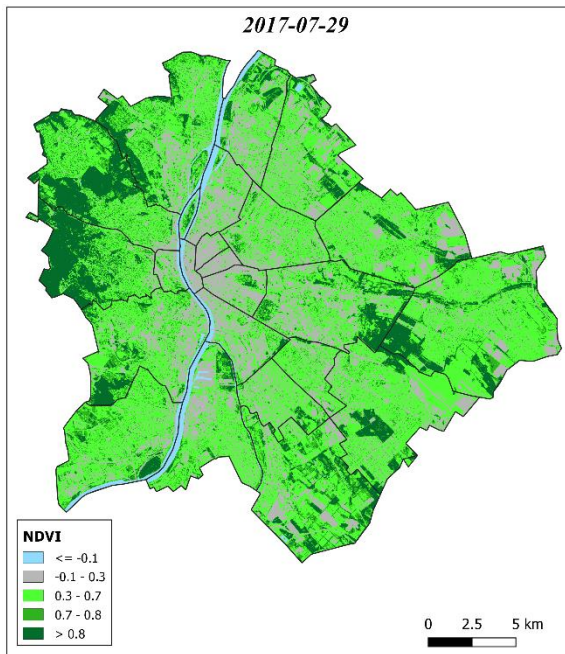


Figure 12. Comparison of NDVI image representation when using different values for Built-up area.

Figure 13, Figure 14, and Figure 15, present two images from each year for five years of NDVI images of Budapest shown in Table 4, which were calculated from the algorithm in Equation 3, after clipping the images to the Budapest borders, they are presented with Geographical projection WGS84/UTM zone 34N.

2017



2018

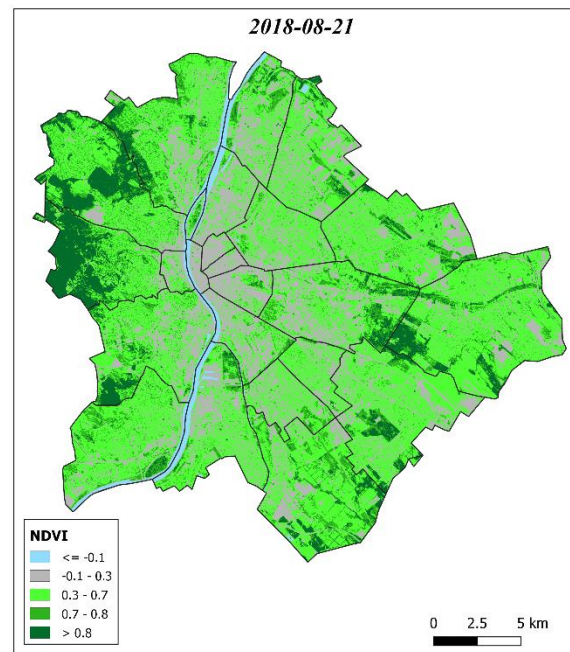
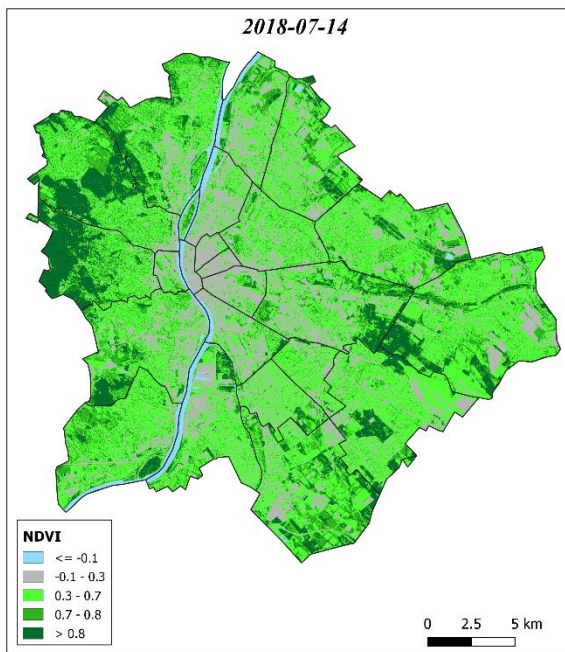
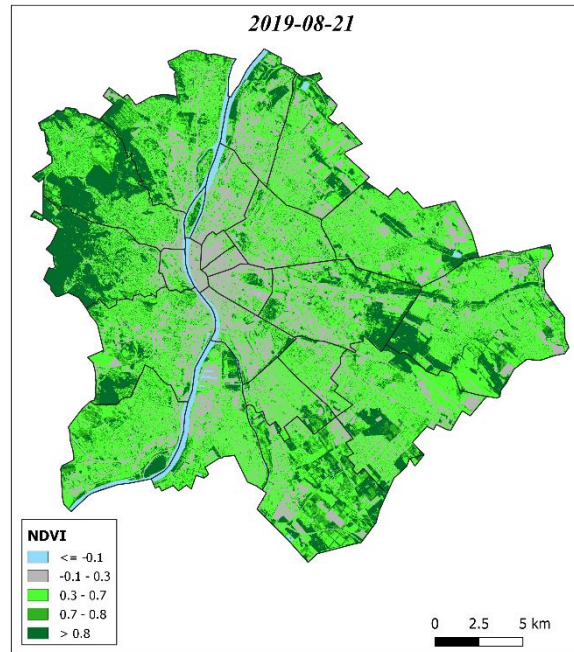
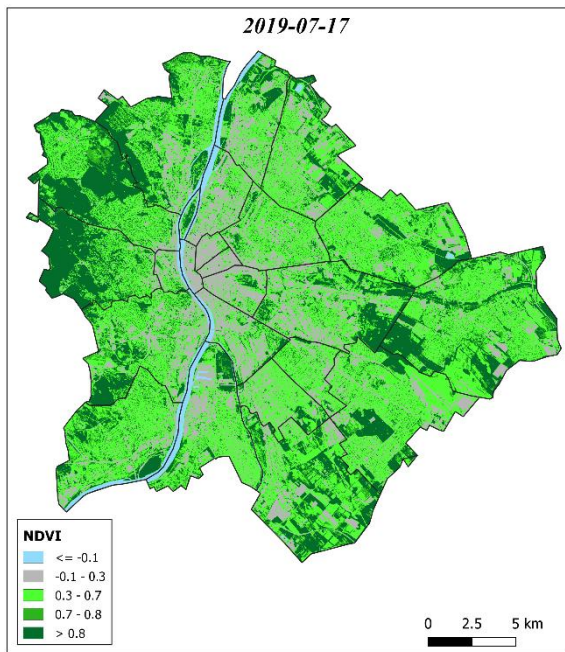


Figure 13. NDVI images for Budapest (1/3).

2019



2020

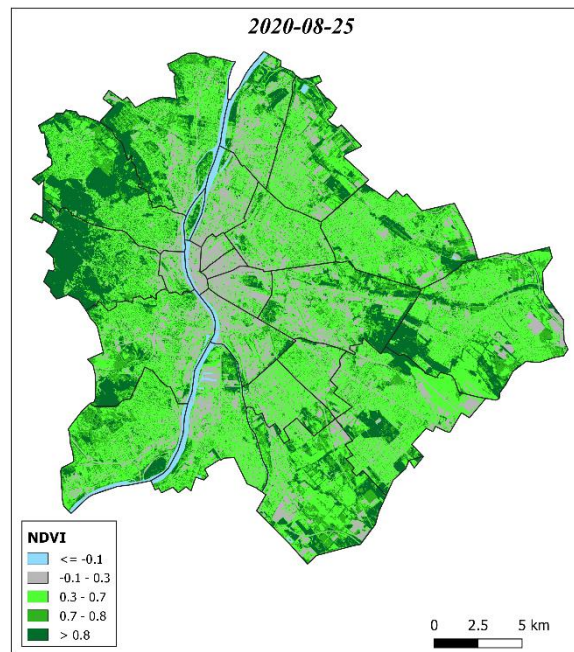
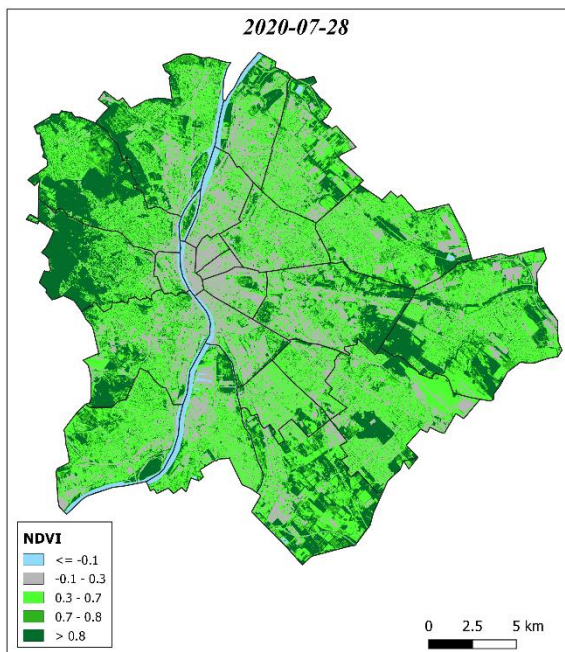


Figure 14. NDVI images for Budapest (2/3).

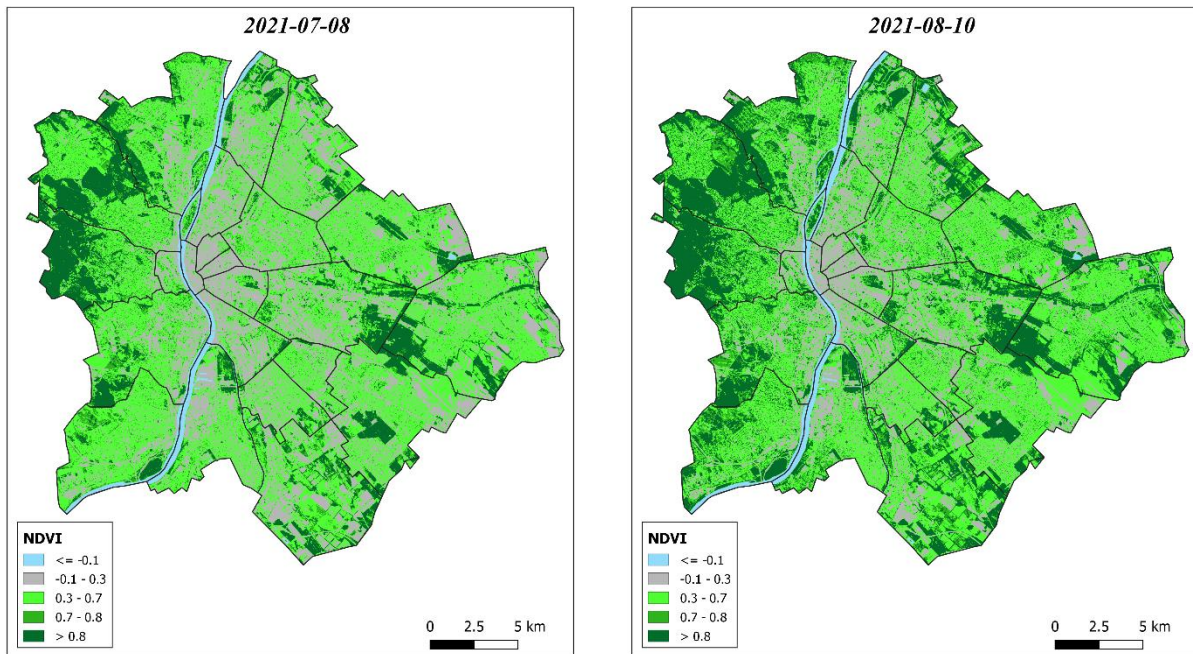


Figure 15. NDVI images for Budapest (3/3).

For this study, the three most green urban areas in the city were selected, which are (Margit-Sziget, Népliget and Városliget), these three areas were studied and the average NDVI was calculated in the 100 m², see Figure 16, Figure 17, and Figure 18.

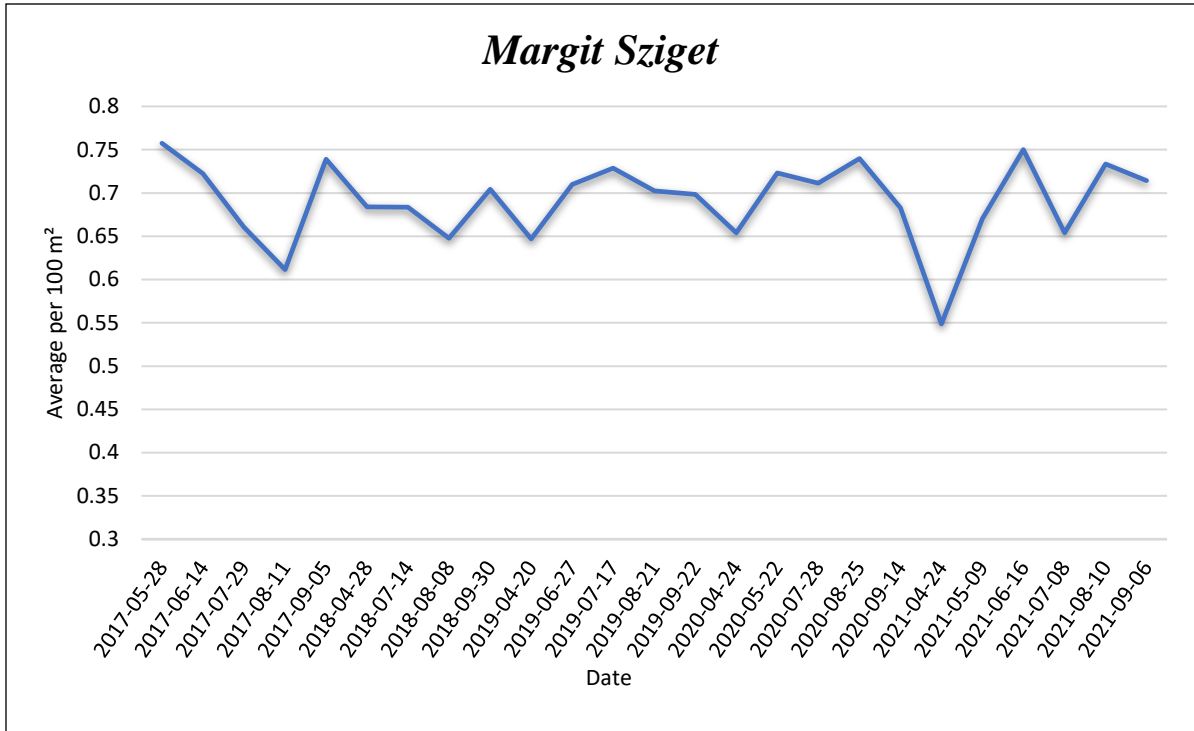


Figure 16. Line chart of NDVI values for Margit Sziget.

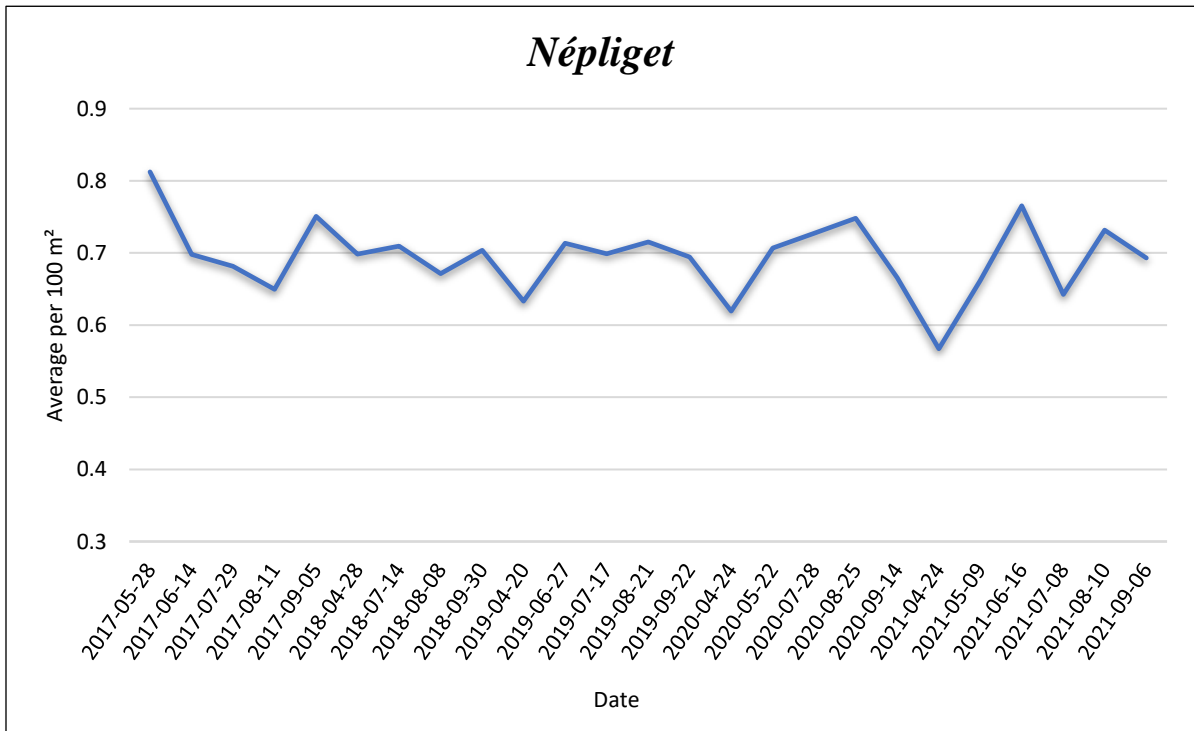


Figure 17. Line chart of NDVI values for Népliget.

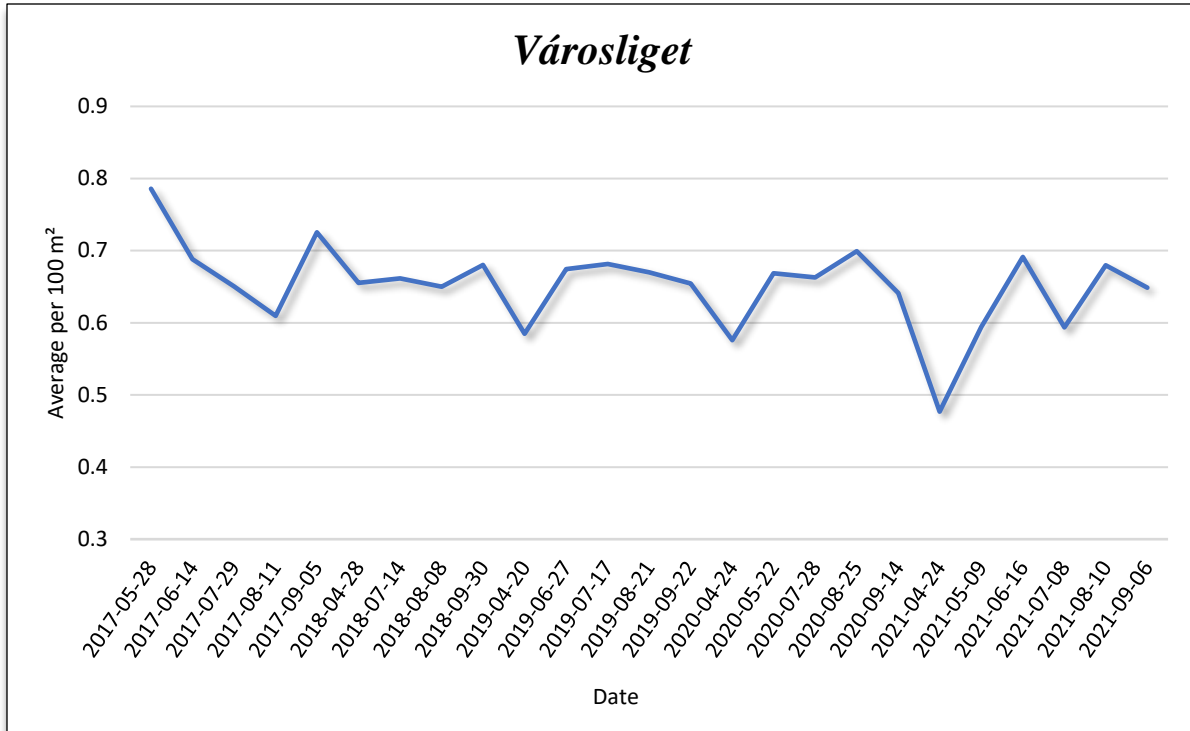


Figure 18. Line chart of NDVI values for Városliget.

A sudden drop in the value of NDVI was observed on 24-04-2021 in particular, and fluctuation in other values in the same year. There is a sharp decrease in the greenness of the image in the month of April, see Figure 19, according to the Hungarian Meteorological Service's annual report, precipitation in Hungary was a little over 500 mm in 2021, over 20% below average, making it one of the driest years, and the average temperature in June and July this year was 22.9 celsius in Hungary, the hottest since 1901.



Figure 19. Variation of vegetation cover between April 2020 and 2021.

And because 2021 is the only year that contains images for all months, a three-dimensional scene has been created for the three areas mentioned, see Figure 20, Figure 21, and Figure 22, for showing an aesthetic character in the display and making it easier to observe the differences between them.

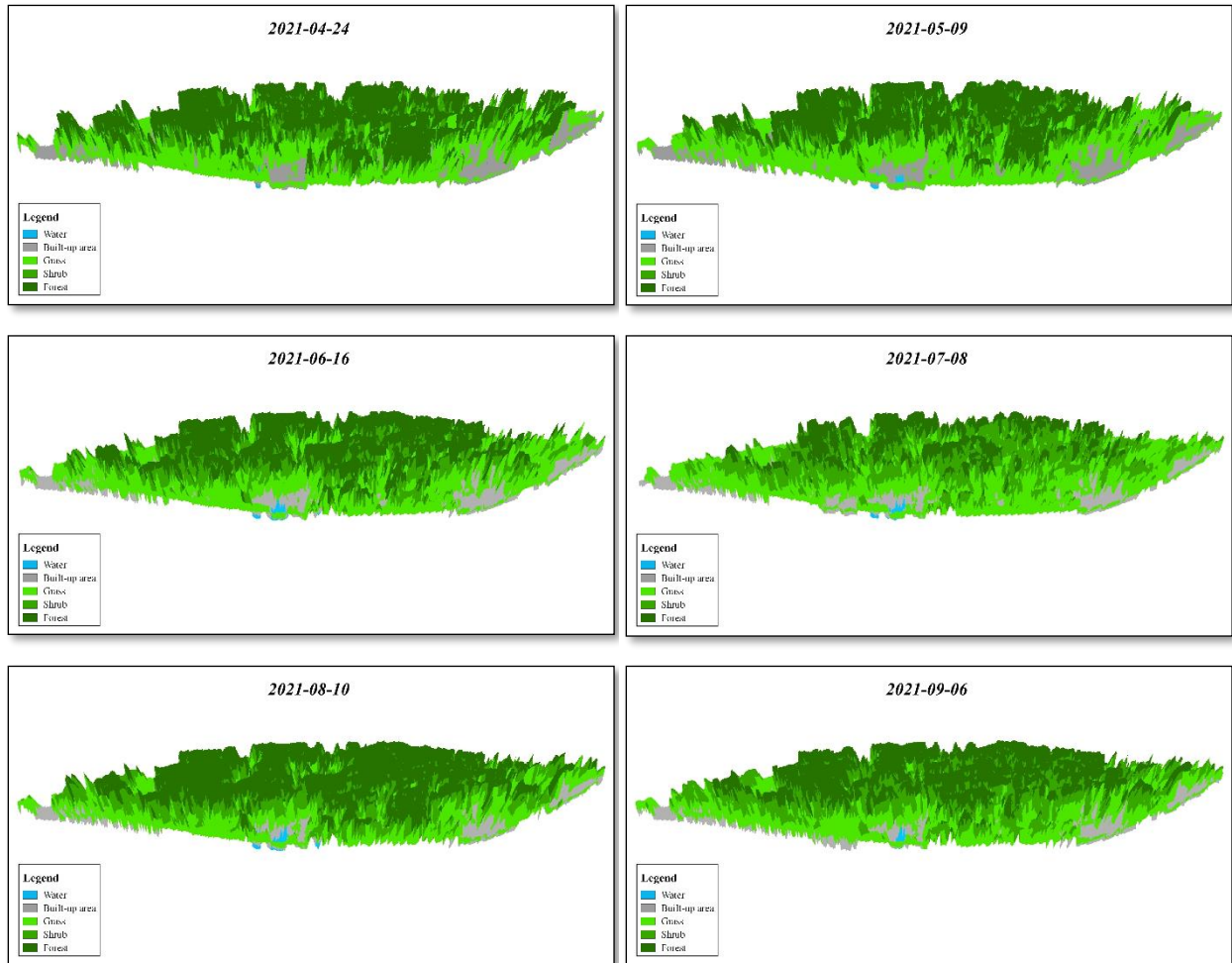


Figure 20. 3D model of NDVI values for Margit Sziget.

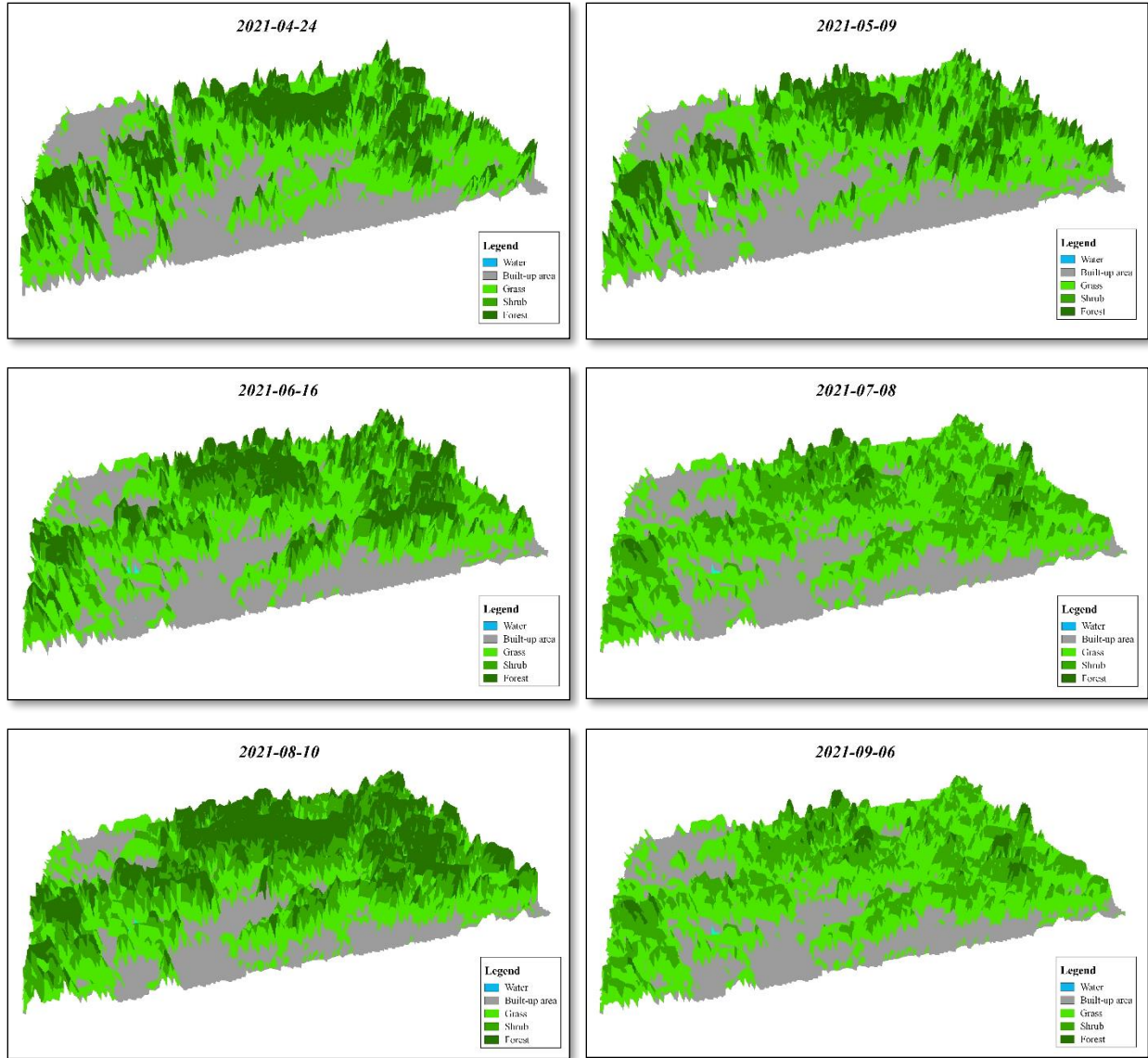


Figure 21. 3D model of NDVI values for Népliget.

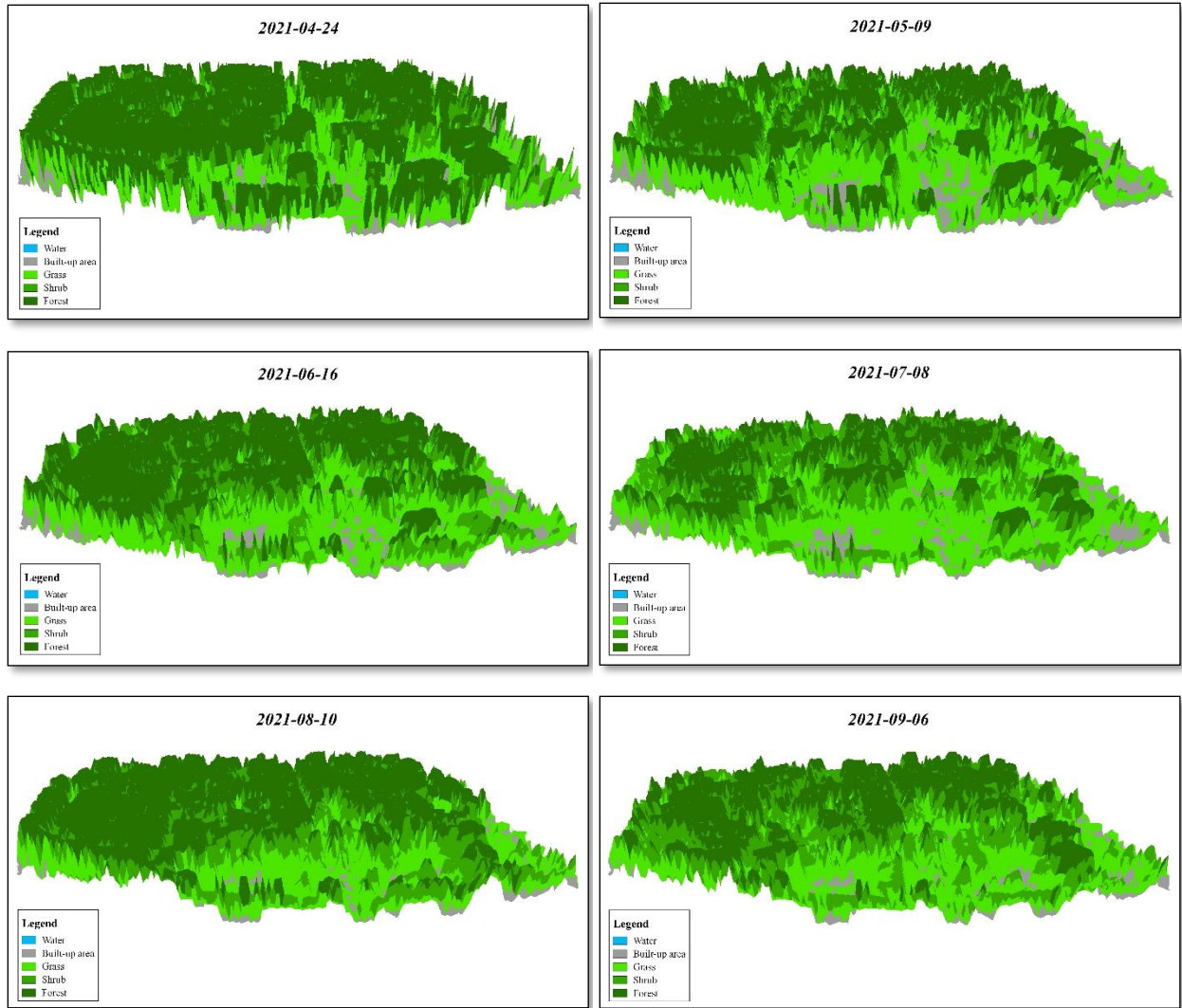


Figure 22. 3D model of NDVI values for Városliget.

4.2. Classification

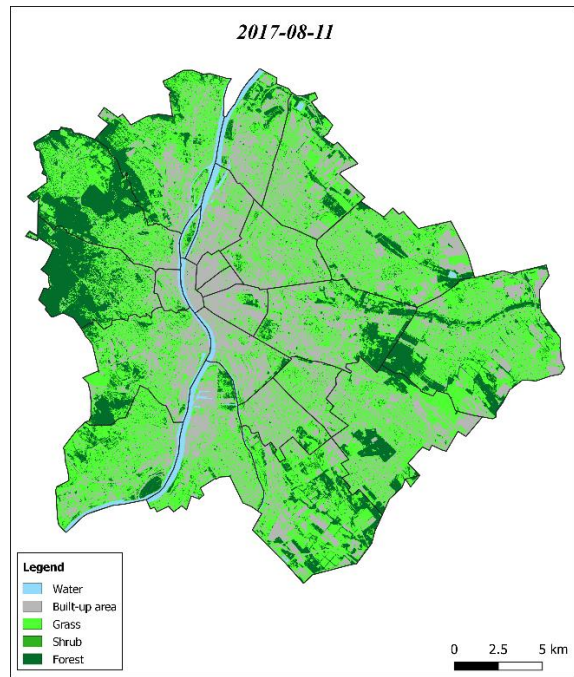
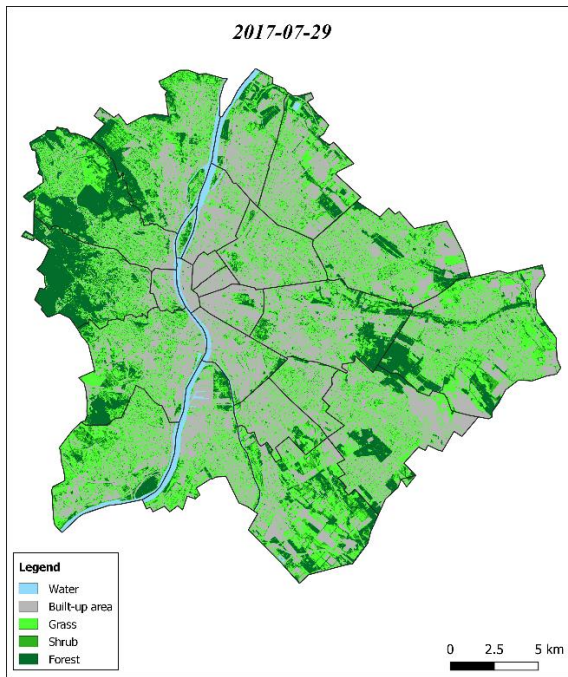
After re-classifying the NDVI images into 5 classes, see Table 9, the training data were created by manually drawing the polygons for each class as shown in Table 6, to perform the supervised classification.

Table 9. Classes of the reclassified NDVI images.

NDVI value	Reclassified NDVI
-1 to -0.1	1
-0.1 to 0.3	2
0.3 to 0.7	3
0.7 to 0.8	4
0.8 to 1	5

Figure 23, Figure 24, and Figure 25, present two images of each year for the five years of the NDVI-based classification images shown in Table 4, and are presented with geographic projection WGS84 / UTM zone 34N.

2017



2018

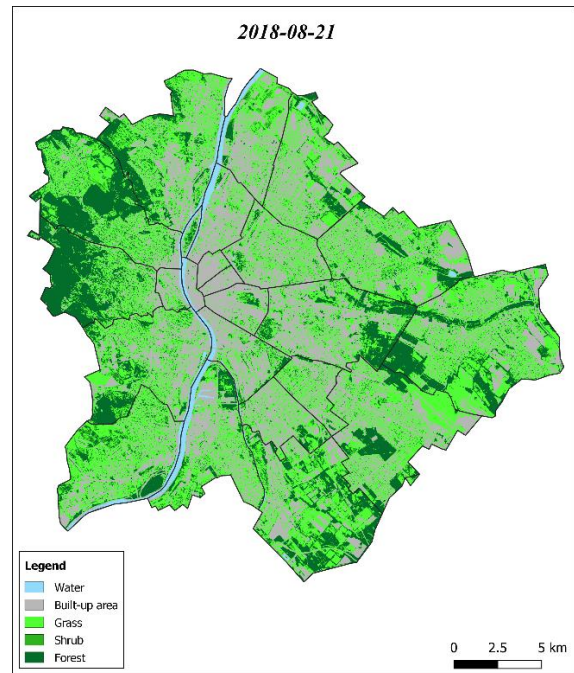
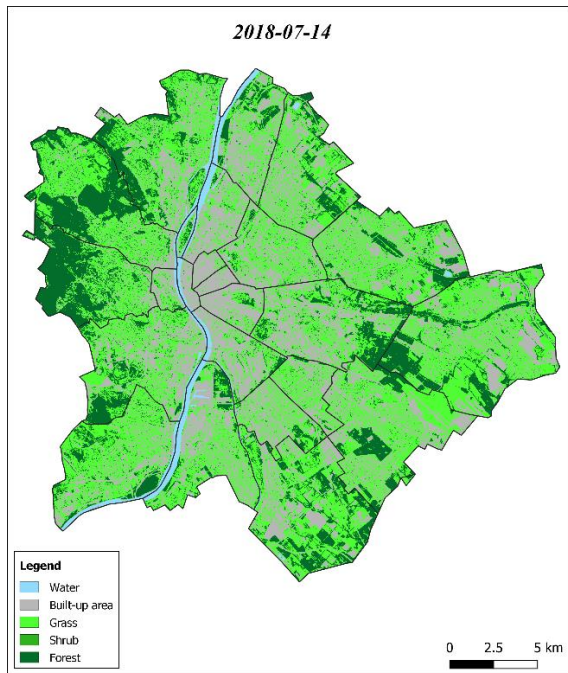
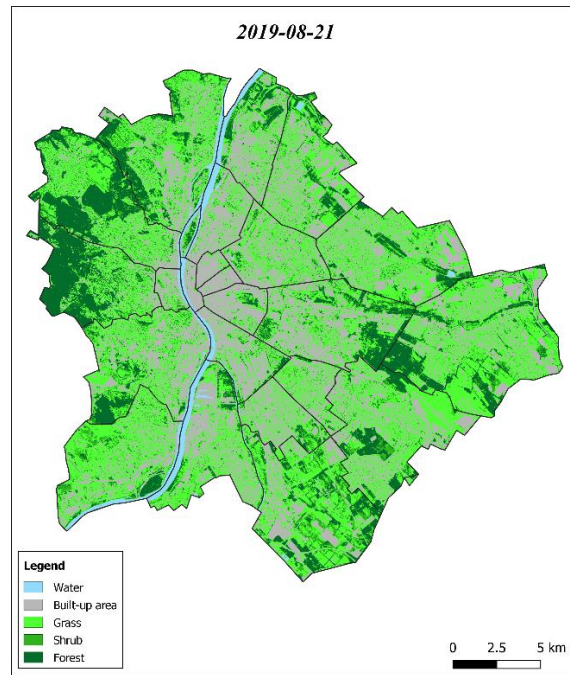
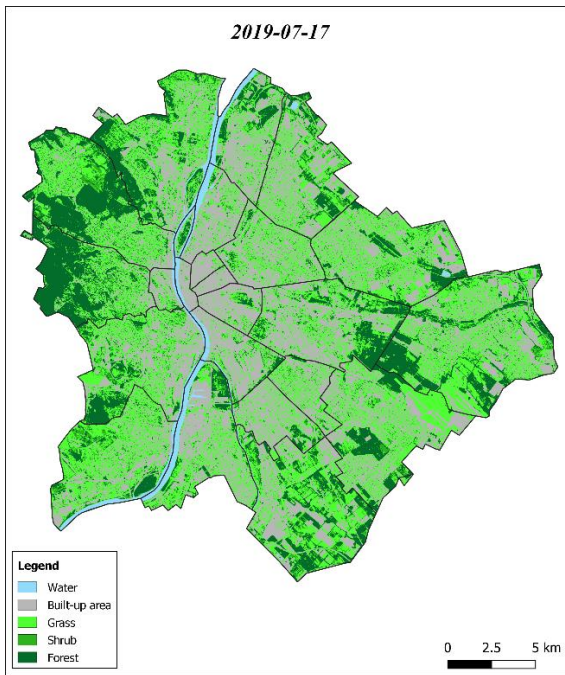


Figure 23. Classified images based on NDVI images for Budapest. (1/3).

2019



2020

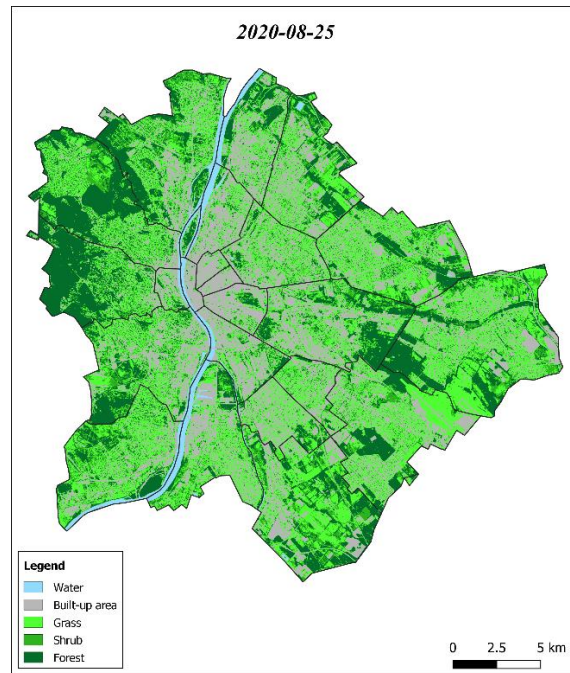
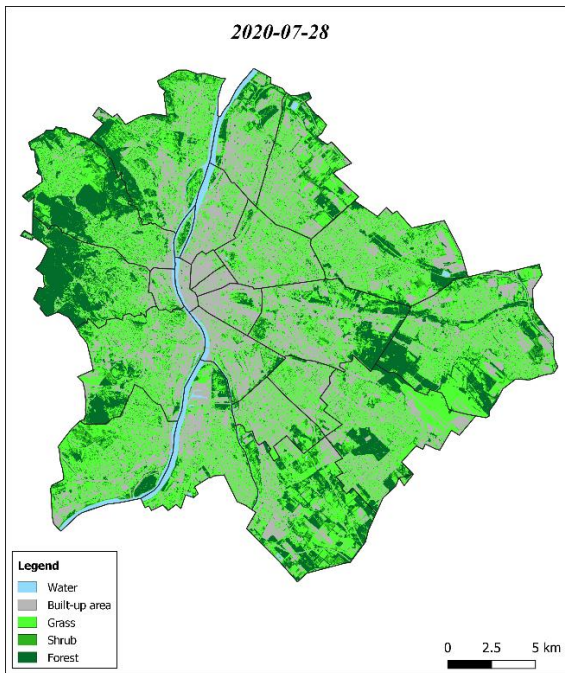


Figure 24. Classified images based on NDVI images for Budapest. (2/3).

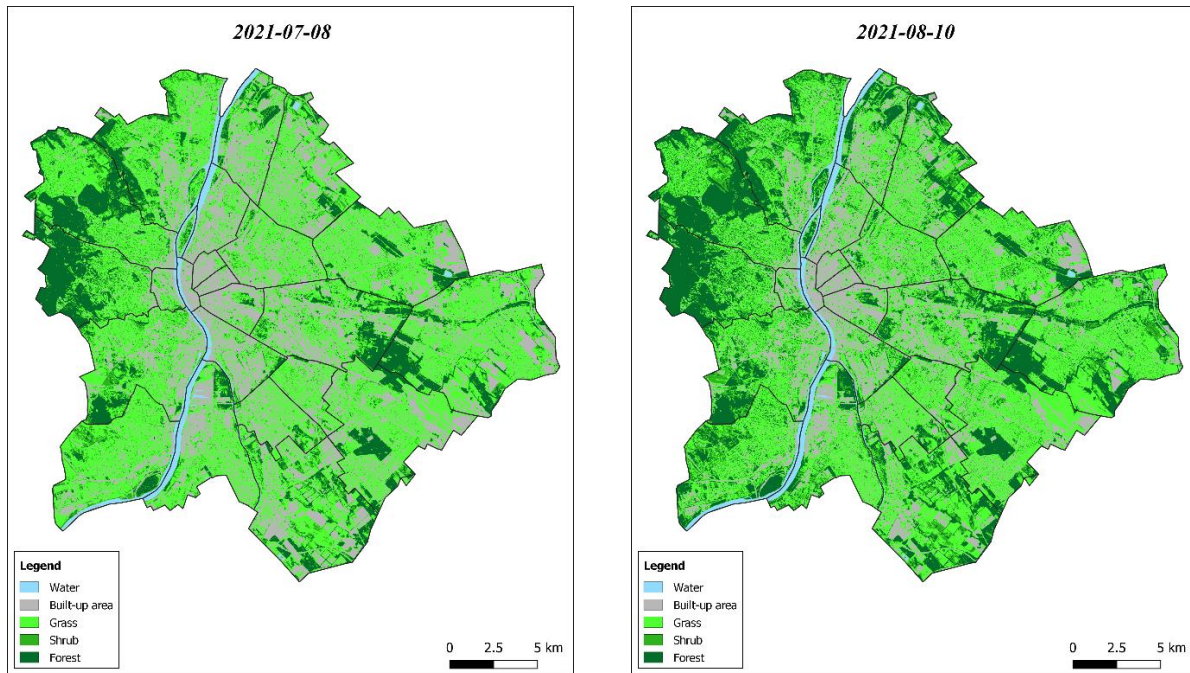


Figure 25. Classified images based on NDVI images for Budapest. (3/3).

4.3. Accuracy assessment

The kappa coefficient was calculated to assess classification accuracy based on manually measured reference points from Google Earth and the results were as shown in the Table 10.

Table 10. Kappa index and overall accuracy.

Year	Month	Day	Kappa Index	Overall accuracy
2017	May	28	0.79	0.83
	June	14	0.72	0.78
	July	29	0.81	0.85
	August	11	0.79	0.83
	September	5	0.83	0.86
2018	April	28	0.85	0.88
	July	14	0.96	0.97
	August	8	0.84	0.87
	September	30	0.74	0.79
2019	April	20	0.62	0.7
	June	27	0.81	0.85
	July	17	0.89	0.91
	August	21	0.8	0.84
	September	22	0.73	0.78
2020	April	24	0.67	0.74
	May	22	0.79	0.83
	July	28	0.95	0.96
	August	25	0.79	0.83
	September	14	0.83	0.86
2021	April	24	0.57	0.66
	May	9	0.78	0.82
	June	16	0.76	0.81
	July	8	0.94	0.95
	August	10	0.83	0.86
	September	6	0.93	0.95

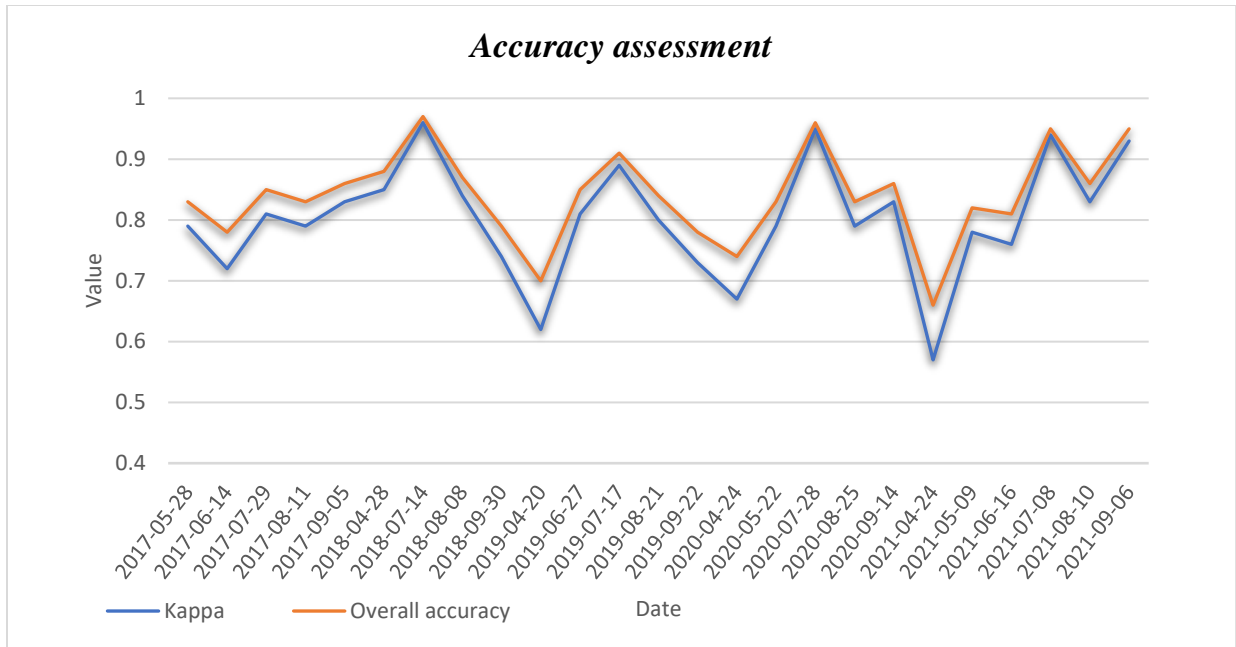


Figure 26. Line chart of the Kappa index and Overall accuracy.

Based on Table 6, all kappa values were good, which indicates a good agreement between the classified images and the reference data, except for one which is April 2021, based on the dry year and the lack of greenness in this year, see Figure 19. Table 11 shows the confusion matrix for April 2021, where it is observed that the decrease in kappa is due to errors in matching the forest, shrub and grass classes where there is a large error rate, which results from poor vegetation cover in that month.

Table 11. Confusion Matrix for April 2021.

		Reference Data				
		Water	Built-up area	Grass	Shrub	Forest
Classified Data	Class					
	Water	15	0	0	0	0
	Built-up area	1	27	0	0	0
	Grass	0	1	10	0	8
	Shrub	0	1	3	6	9
Forest	0	0	7	4	8	

4.4. Land change detection

Based on the fact that the images of the month of July are available in all years, the detection of the land change every year with the following year was performed in the month of July. Table 12 shows the land change for the years mentioned.

Moreover, land change detection was performed between June 2017 and 2021 see Table 12, so that it would be possible to judge whether the percentage of vegetation cover in Budapest has increased or decreased during these years.

Based on what Table 12 shows, Vegetation cover increased in 2021 compared to 2017 by 2.31%, on the other hand, there was a decrease in vegetation cover by 2.12%. As a result, it can be said that Budapest became greener in 2021 compared to 2017 by 1.91 ‰, and as an area, Budapest became greener by 100.35 ha.

Table 12. Land change proportion.

Date	Change type	Land change in each class %	Land change range %
2017 - 2018	Vegetation to Non-Vegetation	1.22	5.08
	Non-Vegetation to Vegetation	3.86	
2018 - 2019	Vegetation to Non-Vegetation	2.44	3.26
	Non-Vegetation to Vegetation	0.82	
2019 - 2020	Vegetation to Non-Vegetation	0.86	1.09
	Non-Vegetation to Vegetation	0.23	
2020 - 2021	Vegetation to Non-Vegetation	3.04	3.77
	Non-Vegetation to Vegetation	0.73	
2017 - 2021	Vegetation to Non-Vegetation	2.12	4.43
	Non-Vegetation to Vegetation	2.31	

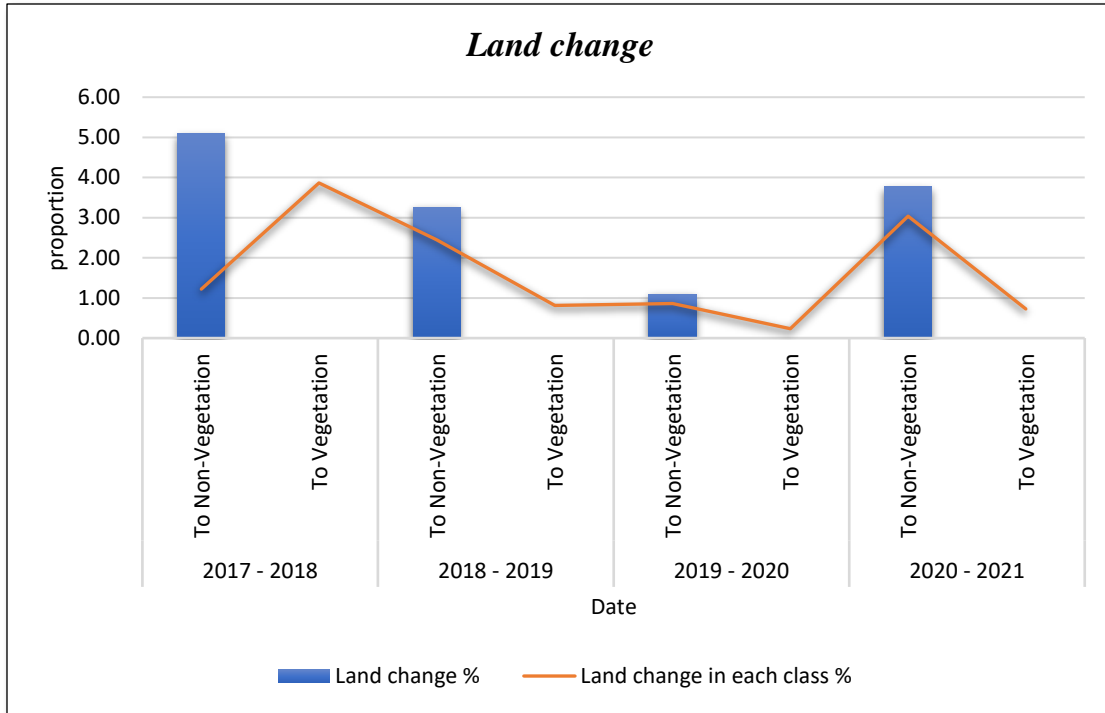


Figure 27. Line chart of land change.

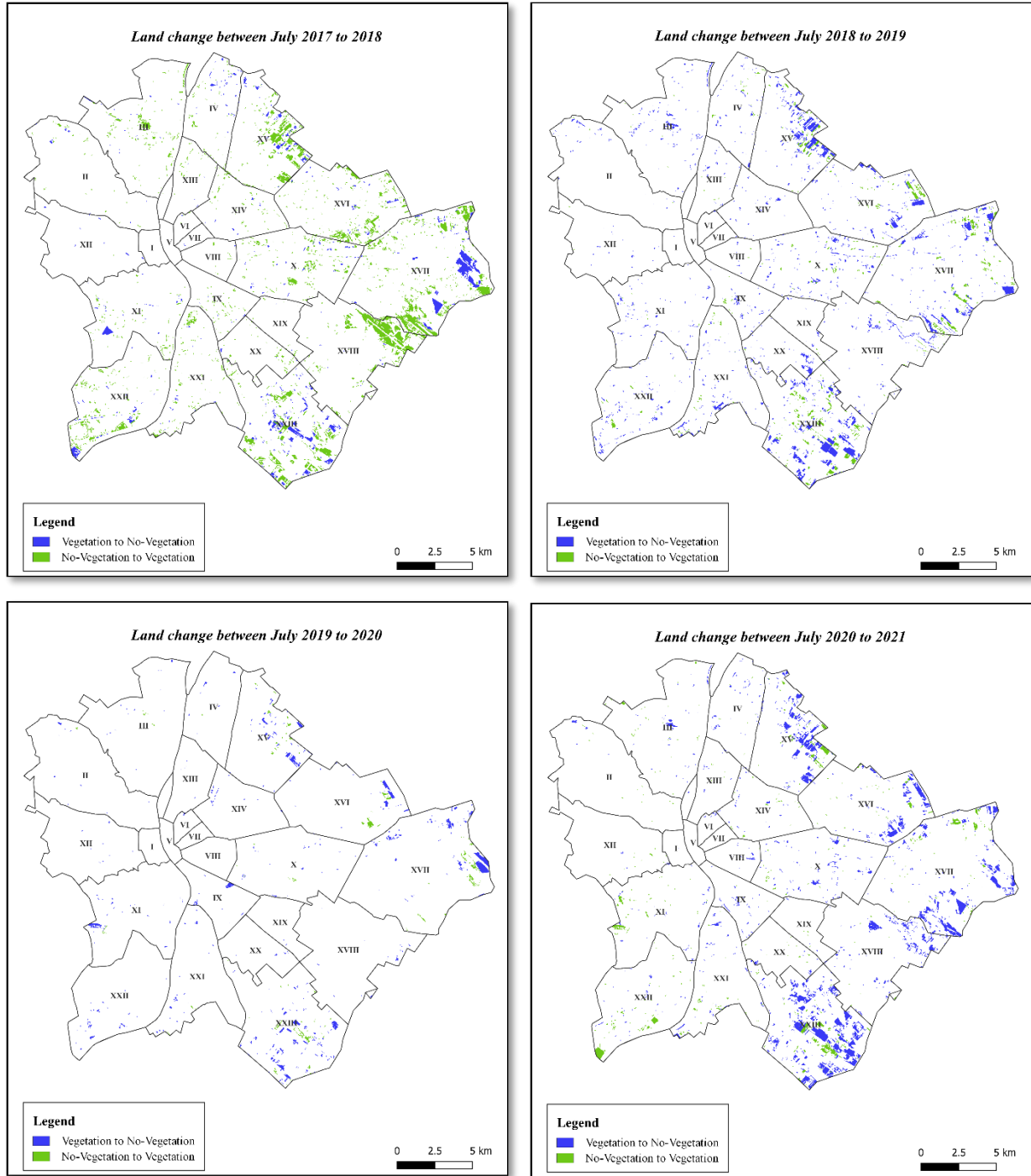


Figure 28. Budapest land change in July between each year and the following year.

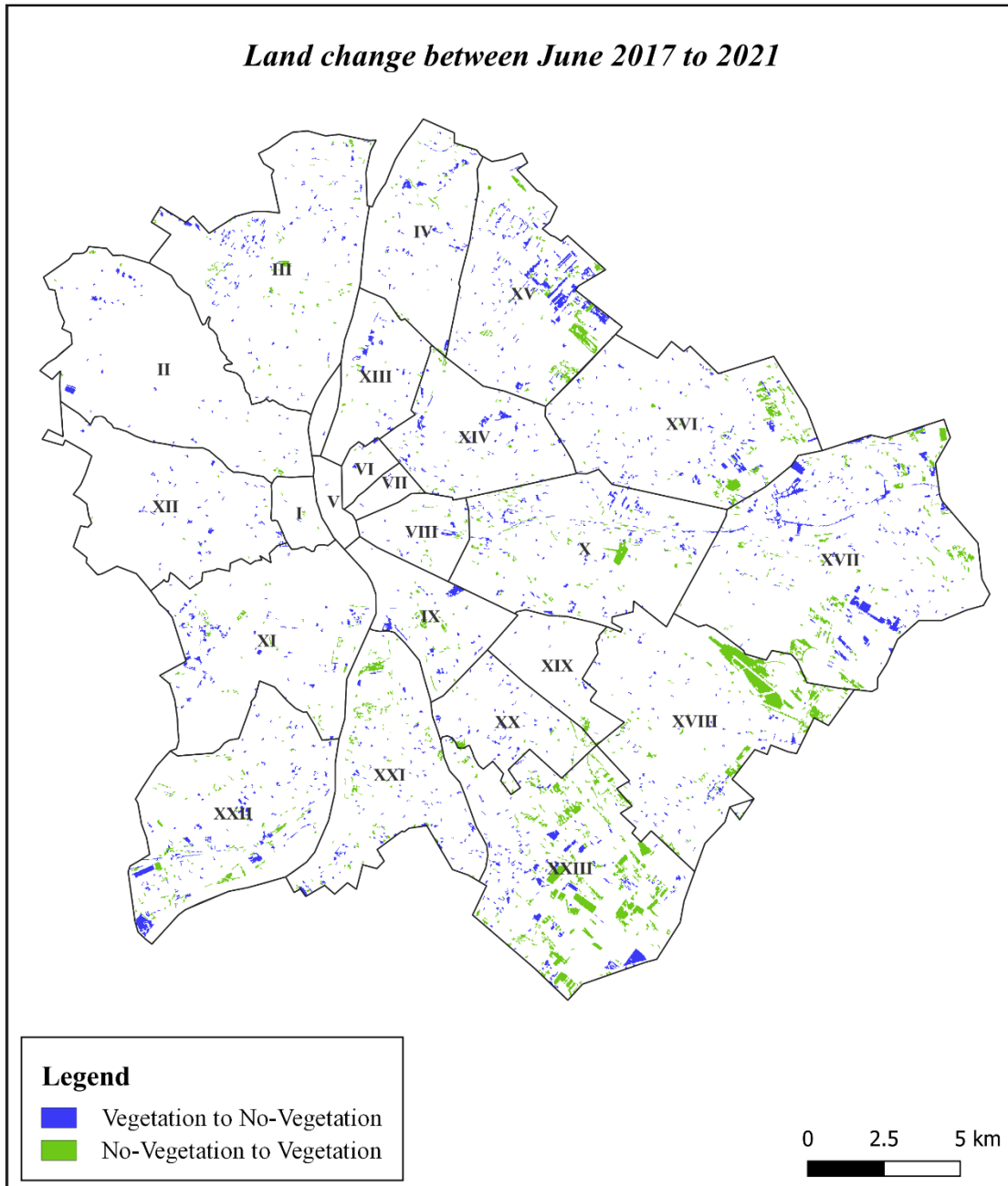


Figure 29. Budapest land change between 2017 to 2021 June.

The districts of Budapest were studied in terms of changes. Figure 30, shows the changes for all districts. It was observed that only six districts became greener. Table 13, Table 14, shows the values for the top three districts, where the XXIII (23) district was the most district has become greener.

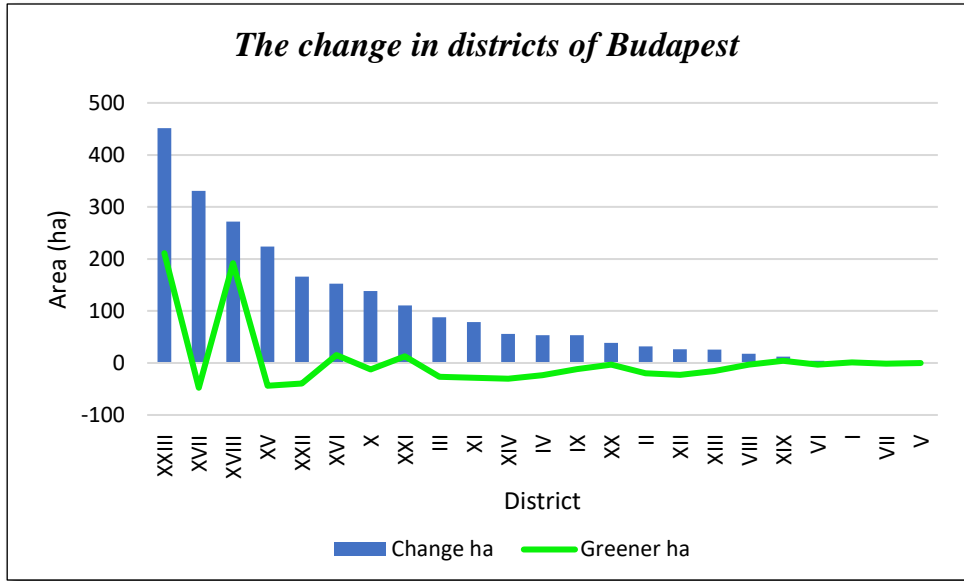


Figure 30. Vegetation changes of Budapest districts.

Table 13. Changes in the top three districts in Budapest.

District	Change (ha)
XXIII	451.35
XVII	330.94
XVIII	271.7

Table 14. Changes in the top three districts that have become greener in Budapest.

District	Became greener (ha)
XXIII	211.07
XVIII	191.68
XVI	15.02

5. Conclusion

Remote sensing is a very effective tool for monitoring vegetation cover quickly and effectively over large areas. In this study, the calculated normalized difference vegetation index (NDVI) values from the Sentinel-2 images with a resolution of 10 meters were relied upon, to study and assess the vegetation cover of Budapest. As this method has proven its effectiveness in classifying and monitoring types of vegetation cover. Sentinel-2 images are also very suitable for use in such applications. The behavior and change of vegetation cover have been studied extensively for the three most urban green areas in the city, where the year 2021 was generally the lowest year in NDVI values, and this is due to the lack of rain and the high temperature in that year. An effective cloud removal methodology was reached, also the method of NDVI threshold-based supervised classification is very effective for determining vegetation changes. Accuracy was also assessed, and all classified images were good except for one in 2021 due to poor vegetation cover in that year for the reasons mentioned above. As it was concluded that the city of Budapest is greener than before by about 100 hectares, and the district that has become greener is district 18 in Pest.

References

- Abdullah, A. Y. M., Masrur, A., Gani Adnan, M. S., Al Baky, M. A., Hassan, Q. K., & Dewan, A. (2019). Spatio-temporal patterns of land use/land cover change in the heterogeneous coastal region of Bangladesh between 1990 and 2017. *Remote Sensing*, 11(7). <https://doi.org/10.3390/rs11070790>
- Al Shaikh, A. Y. (2015). Assessment of the Human Influence on Vegetation Cover Condition Based on Ndvi in Hail, North {KSA}. *Advances in Environmental Biology*, 9(June), 62–73. <http://www.aensiweb.net/AENSIWEB/aeb/aeb/2015/June/62-73.pdf>
- Arévalo, P., Bullock, E. L., Woodcock, C. E., & Olofsson, P. (2020). A Suite of Tools for Continuous Land Change Monitoring in Google Earth Engine. *Frontiers in Climate*, 2(December), 1–19. <https://doi.org/10.3389/fclim.2020.576740>
- Bartholy, J., Dian, C., Pongrácz, R., & Dezsó, Z. (2020). Annual and monthly analysis of surface urban heat island intensity with respect to the local climate zones in Budapest. *Urban Climate*, 31(December 2019), 100573. <https://doi.org/10.1016/j.uclim.2019.100573>
- Belgiu, M., & Drăgu, L. (2016). Random forest in remote sensing: A review of applications and future directions. *ISPRS Journal of Photogrammetry and Remote Sensing*, 114, 24–31. <https://doi.org/10.1016/j.isprsjprs.2016.01.011>
- Boret, F., & Cesaro, J. (2019). *Mapping Amu Darya ' s ecosystem riverbanks : land cover evolution 1988-2018 Report by.* 1–34.
- Breiman, L. (2001). Random Forests. *Lecture Notes in Computer Science (Including Subseries Lecture Notes in Artificial Intelligence and Lecture Notes in Bioinformatics)*, 12343 LNCS, 503–515. https://doi.org/10.1007/978-3-030-62008-0_35
- Brumbaugh, F. (1996). NDWI A Normalized Difference Water Index for Remote Sensing of Vegetation Liquid Water From Space. *Journal of Experimental Education*, 23(4), 359–363. <https://doi.org/10.1080/00220973.1955.11010524>
- Buzási, A. (2022). Comparative assessment of heatwave vulnerability factors for the districts of Budapest, Hungary. *Urban Climate*, 42(February), 101127.

<https://doi.org/10.1016/j.uclim.2022.101127>

- Chavez, P. S. (1996). Image-based atmospheric corrections - Revisited and improved. *Photogrammetric Engineering and Remote Sensing*, 62(9), 1025–1036.
- Churkina, G., Brown, D. G., & Keoleian, G. (2010). Carbon stored in human settlements: The conterminous United States. *Global Change Biology*, 16(1), 135–143. <https://doi.org/10.1111/j.1365-2486.2009.02002.x>
- Chuvieco, E., & Huete, A. (2009). Fundamentals of satellite remote sensing. In *Fundamentals of Satellite Remote Sensing*. <https://doi.org/10.1201/b18954>
- Congalton, R. G. (1991). A review of assessing the accuracy of classifications of remotely sensed data. *Remote Sensing of Environment*, 37(1), 35–46. [https://doi.org/10.1016/0034-4257\(91\)90048-B](https://doi.org/10.1016/0034-4257(91)90048-B)
- Daryaei, A., Sohrabi, H., Atzberger, C., & Immitzer, M. (2020). Fine-scale detection of vegetation in semi-arid mountainous areas with focus on riparian landscapes using Sentinel-2 and UAV data. *Computers and Electronics in Agriculture*, 177(July), 105686. <https://doi.org/10.1016/j.compag.2020.105686>
- Dickinson, D. C., & Hobbs, R. J. (2017). Cultural ecosystem services: Characteristics, challenges and lessons for urban green space research. *Ecosystem Services*, 25, 179–194. <https://doi.org/10.1016/j.ecoser.2017.04.014>
- Dong, P., & Chen, Q. (2017). *LiDAR Remote Sensing and Applications*.
- El-mezouar, M. C., Taleb, N., Kpalma, K., Ronsin, J., El-mezouar, M. C., Taleb, N., Kpalma, K., & A, J. R. (2011). A high-resolution index for vegetation extraction in IKONOS images To cite this version : HAL Id : hal-00582904 A high-resolution index for vegetation extraction in IKONOS images.
- ESA. (2020). *Radiometric Resolutions Sentinel-2 MSI User Guides Sentinel Online [Governmental]*. <https://sentinels.copernicus.eu/web/sentinel/user-guides/sentinel-2-msi/resolutions/radiometric%0A>
- ESA. (2022). *sentinel - 2*. <https://sentinel.esa.int/web/sentinel/missions/sentinel-2>

- ESAb. (2020). *Level-1C Product Formatting Sentinel-2 MSI User Guides Sentinel Online [Governmental]*. <https://sentinels.copernicus.eu/web/sentinel/technical-guides/sentinel-2-msi/level-1c/product-formatting>
- ESAc. (2020). *SNAP Supported Plugins Sen2Cor [Governmental]*. <https://step.esa.int/main/snap-supported-plugins/sen2cor/>
- Foody, G. M. (2002). Status of land cover classification accuracy assessment. *Springer Geography*, 80, 185–201. https://doi.org/10.1007/978-981-16-5149-6_6
- Forkuor, G., & Cofie, O. (2011). Dynamics of land-use and land-cover change in Freetown, Sierra Leone and its effects on urban and peri-urban agriculture - a remote sensing approach. *International Journal of Remote Sensing*, 32(4), 1017–1037. <https://doi.org/10.1080/01431160903505302>
- Gábor, P., & Jombach, S. (2010). The relation between the biological activity and the land surface temperature in Budapest. *Applied Ecology and Environmental Research*, 7(3), 241–251. https://doi.org/10.15666/aeer/0703_241251
- Gao, G., & Gu, Y. (2017). Multitemporal landsat missing data recovery based on tempo-spectral angle model. *IEEE Transactions on Geoscience and Remote Sensing*, 55(7), 3656–3668. <https://doi.org/10.1109/TGRS.2017.2656162>
- Gibbs, H. K., Brown, S., Niles, J. O., & Foley, J. A. (2007). Monitoring and estimating tropical forest carbon stocks: Making REDD a reality. *Environmental Research Letters*, 2(4). <https://doi.org/10.1088/1748-9326/2/4/045023>
- Gren, Å., Barton, D. N., & Langemeyer, O. (2013). Urbanization, biodiversity and ecosystem services: Challenges and opportunities: A global assessment. In *Urbanization, Biodiversity and Ecosystem Services: Challenges and Opportunities: A Global Assessment* (Issue June 2016). <https://doi.org/10.1007/978-94-007-7088-1>
- Hancock, S., Anderson, K., Disney, M., & Gaston, K. J. (2017). Measurement of fine-spatial-resolution 3D vegetation structure with airborne waveform lidar: Calibration and validation with voxelised terrestrial lidar. *Remote Sensing of Environment*, 188, 37–50. <https://doi.org/10.1016/j.rse.2016.10.041>

- Hecht, R., Meinel, G., & Buchroithner, M. F. (2008). Estimation of urban green volume based on single-pulse LiDAR data. *IEEE Transactions on Geoscience and Remote Sensing*, 46(11), 3832–3840. <https://doi.org/10.1109/TGRS.2008.2001771>
- Hu, T., Yang, J., Li, X., & Gong, P. (2016). Mapping urban land use by using landsat images and open social data. *Remote Sensing*, 8(2). <https://doi.org/10.3390/rs8020151>
- Huang, S., Tang, L., Hupy, J. P., Wang, Y., & Shao, G. (2021). A commentary review on the use of normalized difference vegetation index (NDVI) in the era of popular remote sensing. *Journal of Forestry Research*, 32(1), 1–6. <https://doi.org/10.1007/s11676-020-01155-1>
- J.J.Wynne, & Jenness, J. (2005). *Cohen's Kappa and classification table metrics 2.0: an ArcView 3.x extension for accuracy assessment of spatially explicit models: U.S. Geological Survey Open-File Report OF 2005-1363. December, 1–91.* https://www.fs.fed.us/rm/pubs_other/rmrs_2005_jenness_j001.pdf
- Jabbar, M., Yusoff, M. M., & Shafie, A. (2021). Assessing the role of urban green spaces for human well-being: a systematic review. *GeoJournal*, 7. <https://doi.org/10.1007/s10708-021-10474-7>
- Jadhav, J. K., & Singh, R. P. (2018). Automatic semantic segmentation and classification of remote sensing data for agriculture. *Mathematical Models in Engineering*, 4(2), 112–137. <https://doi.org/10.21595/mme.2018.19840>
- Jim, C. Y. (2013). Sustainable urban greening strategies for compact cities in developing and developed economies. *Urban Ecosystems*, 16(4), 741–761. <https://doi.org/10.1007/s11252-012-0268-x>
- Jung, A. (2007). *Application of Airborne Hyperspectral and Thermal Images*. 5(1), 165–175.
- Jung, A., Lausch, A., Bastian, O., Klotz, S., Leitão, P. J., Rocchini, D., Schaepman, M. E., Skidmore, A. K., Tischendorf, L., & Knapp, S. (2018). Understanding and assessing vegetation health by in situ species and remote-sensing approaches. *Methods in Ecology and Evolution*, 9(8), 1799–1809. <https://doi.org/10.1111/2041-210X.13025>
- Jusoff, K., & Senthavy, S. (2003). Land use change detection using remote sensing and geographical information system (GIS) in Gua Musang district, Kelantan, Malaysia. *Journal*

of Tropical Forest Science, 15(2), 303–312.

- Kabisch, N., Strohbach, M., Haase, D., & Kronenberg, J. (2016). Urban green space availability in European cities. *Ecological Indicators*, 70, 586–596. <https://doi.org/10.1016/j.ecolind.2016.02.029>
- Kecman, V. (2005). Support Vector Machines – An Introduction 1 Basics of Learning from Data. *StudFuzz*, 177, 1–47.
- Laaksonen, J., & Oja, E. (1996). Classification with learning k-nearest neighbors. *IEEE International Conference on Neural Networks - Conference Proceedings*, 3, 1480–1483. <https://doi.org/10.1109/icnn.1996.549118>
- Landis, J. R., & Koch, G. G. (1977). The Measurement of Observer Agreement for Categorical Data Published by: International Biometric Society Stable URL : <http://www.jstor.org/stable/2529310>. *Biometrics*, 33(1), 159–174.
- Li, L., Zhou, X., Chen, L., Chen, L., Zhang, Y., & Liu, Y. (2020). Estimating urban vegetation biomass from sentinel-2A image data. *Forests*, 11(2), 1–24. <https://doi.org/10.3390/f11020125>
- Liang, P., Shi, W., & Zhang, X. (2018). Remote sensing image classification based on Stacked Denoising Autoencoder. *Remote Sensing*, 10(1), 1–12. <https://doi.org/10.3390/rs10010016>
- Liang, S., & Wang, J. (2020). *ADVANCED REMOTE SENSING*.
- Liu, Y., Gong, W., Hu, X., & Gong, J. (2018). Forest type identification with random forest using Sentinel-1A, Sentinel-2A, multi-temporal Landsat-8 and DEM data. *Remote Sensing*, 10(6), 1–25. <https://doi.org/10.3390/rs10060946>
- Lorenzi, L., Melgani, F., & Mercier, G. (2013). Missing-area reconstruction in multispectral images under a compressive sensing perspective. *IEEE Transactions on Geoscience and Remote Sensing*, 51(7), 3998–4008. <https://doi.org/10.1109/TGRS.2012.2227329>
- Lu, D. (2006). The potential and challenge of remote sensing-based biomass estimation. *International Journal of Remote Sensing*, 27(7), 1297–1328. <https://doi.org/10.1080/01431160500486732>

- Luo, X., Tong, X., Hu, Z., & Wu, G. (2020). Improving urban land cover/use mapping by integrating a hybrid convolutional neural network and an automatic training sample expanding strategy. *Remote Sensing*, 12(14). <https://doi.org/10.3390/rs12142292>
- Mahajan, U., & Bundel, B. R. (2016). Drones for Normalized Difference Vegetation Index (NDVI), to Estimate Crop Health for Precision Agriculture: A Cheaper Alternative for Spatial Satellite Sensors. *International Conference on Innovative Research in Agriculture, Food Science, Forestry, Horticulture, Aquaculture, Animal Sciences, Biodiversity, Ecological Sciences and Climate Change (AFHABEC-2016)*, January, 38–41.
- Mohd Hasmadi, I., Pakhriazad, H. Z., & Shahrin, M. F. (2009). Evaluating supervised and unsupervised techniques for land cover mapping using remote sensing data. *Malaysia NJournal of Society and Space*, 5(1), 1–10.
- Orhan, O., Ekercin, S., & Dadaser-Celik, F. (2014). Use of Landsat land surface temperature and vegetation indices for monitoring drought in the Salt Lake Basin Area, Turkey. *The Scientific World Journal*, 2014(Vci). <https://doi.org/10.1155/2014/142939>
- Oseni, A. E., Ode, G. ., & Kosoko, A. . (2020). Land use/ land cover classification and change detection mapping: A case study of Lagos state, Nigeria. *International Journal Of Rural Development, Environment And Health Research*, 4(4), 126–144. <https://doi.org/10.22161/ijreh.4.4.2>
- Ozkan, S., Efendioglu, M., & Demirpolat, C. (2018). Cloud detection from RGB color remote sensing images with deep pyramid networks. *International Geoscience and Remote Sensing Symposium (IGARSS)*, 2018-July, 6939–6942. <https://doi.org/10.1109/IGARSS.2018.8519570>
- Páldy, A., Bobvos, J., Vámos, A., Kovats, R. S., & Hajat, S. (2005). The effect of temperature and heat waves on daily mortality in Budapest, Hungary, 1970-2000. *Extreme Weather Events and Public Health Responses, IPCC 2001*, 99–107. https://doi.org/10.1007/3-540-28862-7_10
- Péter, L. (2021). “Budapest”. *Encyclopedia Britannica*. <https://www.britannica.com/place/Budapest>

- Phan, P., Chen, N., Xu, L., & Chen, Z. (2020). Using multi-temporal MODIS NDVI data to monitor tea status and forecast yield: A case study at Tanuyen, Laichau, Vietnam. *Remote Sensing*, 12(11). <https://doi.org/10.3390/rs12111814>
- Pickett, S. T. A., Cadenasso, M. L., Grove, J. M., Boone, C. G., Groffman, P. M., Irwin, E., Kaushal, S. S., Marshall, V., McGrath, B. P., Nilon, C. H., Pouyat, R. V., Szlavecz, K., Troy, A., & Warren, P. (2011). Urban ecological systems: Scientific foundations and a decade of progress. *Journal of Environmental Management*, 92(3), 331–362. <https://doi.org/10.1016/j.jenvman.2010.08.022>
- Pongracz, R., Bartholy, J., Dezso, Z., & Fricke, C. (2016). Analysis of the role of urban vegetation in local climate of Budapest using satellite measurements. *Fourth International Conference on Remote Sensing and Geoinformation of the Environment (RSCy2016)*, 9688, 96881J. <https://doi.org/10.1117/12.2240739>
- Puissant, A., Rougiera, S., & Stumpf, A. (2014). Object-oriented mapping of urban trees using random forest classifiers. *International Journal of Applied Earth Observation and Geoinformation*, 26(1), 235–245. <https://doi.org/10.1016/j.jag.2013.07.002>
- Qian, Y., Zhou, W., Yu, W., & Pickett, S. T. A. (2015). Quantifying spatiotemporal pattern of urban greenspace: new insights from high resolution data. *Landscape Ecology*, 30(7), 1165–1173. <https://doi.org/10.1007/s10980-015-0195-3>
- Sarukkai, V., Jain, A., UzKent, B., & Ermon, S. (2020). Cloud removal in satellite images using spatiotemporal generative networks. *Proceedings - 2020 IEEE Winter Conference on Applications of Computer Vision, WACV 2020*, 1785–1794. <https://doi.org/10.1109/WACV45572.2020.9093564>
- Schultz, G. A., & Engman, E. T. (2000). Remote Sensing in Hydrology and Water Management. In *Remote Sensing in Hydrology and Water Management*. <https://doi.org/10.1007/978-3-642-59583-7>
- Shen, H., Li, X., Cheng, Q., Zeng, C., Yang, G., Li, H., & Zhang, L. (2015). Missing Information Reconstruction of Remote Sensing Data: A Technical Review. *IEEE Geoscience and Remote Sensing Magazine*, 3(3), 61–85. <https://doi.org/10.1109/MGRS.2015.2441912>

- Simmon, R. (2022). *Lead Data Visualizer and Information Designer (NASA)*.
https://earthobservatory.nasa.gov/features/MeasuringVegetation/measuring_vegetation_2.php
- Singh, S. K., & Reddy, G. P. O. (2018). *Geotechnologies and the Environment Geospatial Technologies in Land Resources Mapping, Monitoring and Management*.
<http://www.springer.com/series/8088>
- Sousa, A. M. O., Gonçalves, A. C., Mesquita, P., & Marques da Silva, J. R. (2015). Biomass estimation with high resolution satellite images: A case study of *Quercus rotundifolia*. *ISPRS Journal of Photogrammetry and Remote Sensing*, 101, 69–79.
<https://doi.org/10.1016/j.isprsjprs.2014.12.004>
- Suab, S. A., & Avtar, R. (2020). Unmanned Aerial Vehicle System (UAVS) Applications in Forestry and Plantation Operations: Experiences in Sabah and Sarawak, Malaysian Borneo. In *Unmanned Aerial Vehicle: Applications in Agriculture and Environment*.
https://doi.org/10.1007/978-3-030-27157-2_8
- Subramaniam, A., & Mallast, U. (2017). *Remote Sensing Class*. <https://www.baltic-transcoast.uni-rostock.de/news/news-2020-2017/remote-sensing-class-2017/>
- Tan, P. Y., Wang, J., & Sia, A. (2013). Perspectives on five decades of the urban greening of Singapore. *Cities*, 32, 24–32. <https://doi.org/10.1016/j.cities.2013.02.001>
- Taufik, A., Syed Ahmad, S. S., & Azmi, E. F. (2019). Classification of landsat 8 satellite data using unsupervised methods. *Lecture Notes in Networks and Systems*, 67(January), 275–284.
https://doi.org/10.1007/978-981-13-6031-2_46
- Tempa, K., & Aryal, K. R. (2022). Semi-automatic classification for rapid delineation of the geohazard-prone areas using Sentinel-2 satellite imagery. *SN Applied Sciences*, 4(5).
<https://doi.org/10.1007/s42452-022-05028-6>
- Tewabe, D., & Fentahun, T. (2020). Assessing land use and land cover change detection using remote sensing in the Lake Tana Basin, Northwest Ethiopia. *Cogent Environmental Science*, 6(1). <https://doi.org/10.1080/23311843.2020.1778998>
- Timilsina, S., Aryal, J., & Kirkpatrick, J. B. (2020). Mapping urban tree cover changes using

- object-based convolution neural network (OB-CNN). *Remote Sensing*, 12(18).
<https://doi.org/10.3390/RS12183017>
- Uçar, Z., Akay, A. E., & Bilici, E. (2020). Towards green smart cities: Importance of Urban forestry and urban vegetation. *International Archives of the Photogrammetry, Remote Sensing and Spatial Information Sciences - ISPRS Archives*, 44(4/W3), 399–403.
<https://doi.org/10.5194/isprs-archives-XLIV-4-W3-2020-399-2020>
- Venter, Z. S., Barton, D. N., Gundersen, V., Figari, H., & Nowell, M. (2020). Urban nature in a time of crisis: Recreational use of green space increases during the COVID-19 outbreak in Oslo, Norway. *Environmental Research Letters*, 15(10). <https://doi.org/10.1088/1748-9326/abb396>
- Wegner, J. D., Branson, S., Hall, D., Schindler, K., & Perona, P. (2016). Cataloging public objects using aerial and street-level images - Urban trees. *Proceedings of the IEEE Computer Society Conference on Computer Vision and Pattern Recognition, 2016-Decem*, 6014–6023.
<https://doi.org/10.1109/CVPR.2016.647>
- Wilson, E. H., & Sader, S. A. (2002). Detection of forest harvest type using multiple dates of Landsat TM imagery. *Remote Sensing of Environment*, 80(3), 385–396.
[https://doi.org/10.1016/S0034-4257\(01\)00318-2](https://doi.org/10.1016/S0034-4257(01)00318-2)
- Xing, X., Yan, C., Jia, Y., Jia, H., Lu, J., & Luo, G. (2020). An effective high spatiotemporal resolution ndvi fusion model based on histogram clustering. *Remote Sensing*, 12(22), 1–21.
<https://doi.org/10.3390/rs12223774>
- Ya'Acob, N., Azize, A. B. M., Mahmon, N. A., Yusof, A. L., Azmi, N. F., & Mustafa, N. (2014). Temporal forest change detection and forest health assessment using remote sensing. *IOP Conference Series: Earth and Environmental Science*, 19(1). <https://doi.org/10.1088/1755-1315/19/1/012017>
- Zaitunah, A., Samsuri, S., Ahmad, A. G., & Safitri, R. A. (2018). Normalized difference vegetation index (ndvi) analysis for land cover types using landsat 8 oli in besitang watershed, Indonesia. *IOP Conference Series: Earth and Environmental Science*, 126(1).
<https://doi.org/10.1088/1755-1315/126/1/012112>

- Zhang, H., Zhang, X., & Shu, N. (2009). Study on Land Use Cover Change (LUCC) based on remote sensing and GIS. *International Symposium on Spatial Analysis, Spatial-Temporal Data Modeling, and Data Mining*, 7492, 749202. <https://doi.org/10.1117/12.838274>
- Zhang, J., Clayton, M. K., & Townsend, P. A. (2015). Missing data and regression models for spatial images. *IEEE Transactions on Geoscience and Remote Sensing*, 53(3), 1574–1582. <https://doi.org/10.1109/TGRS.2014.2345513>
- Zhang, Y., Wen, F., Gao, Z., & Ling, X. (2019). A Coarse-to-Fine Framework for Cloud Removal in Remote Sensing Image Sequence. *IEEE Transactions on Geoscience and Remote Sensing*, 57(8), 5963–5974. <https://doi.org/10.1109/TGRS.2019.2903594>

ANNEX

NDVI

2017

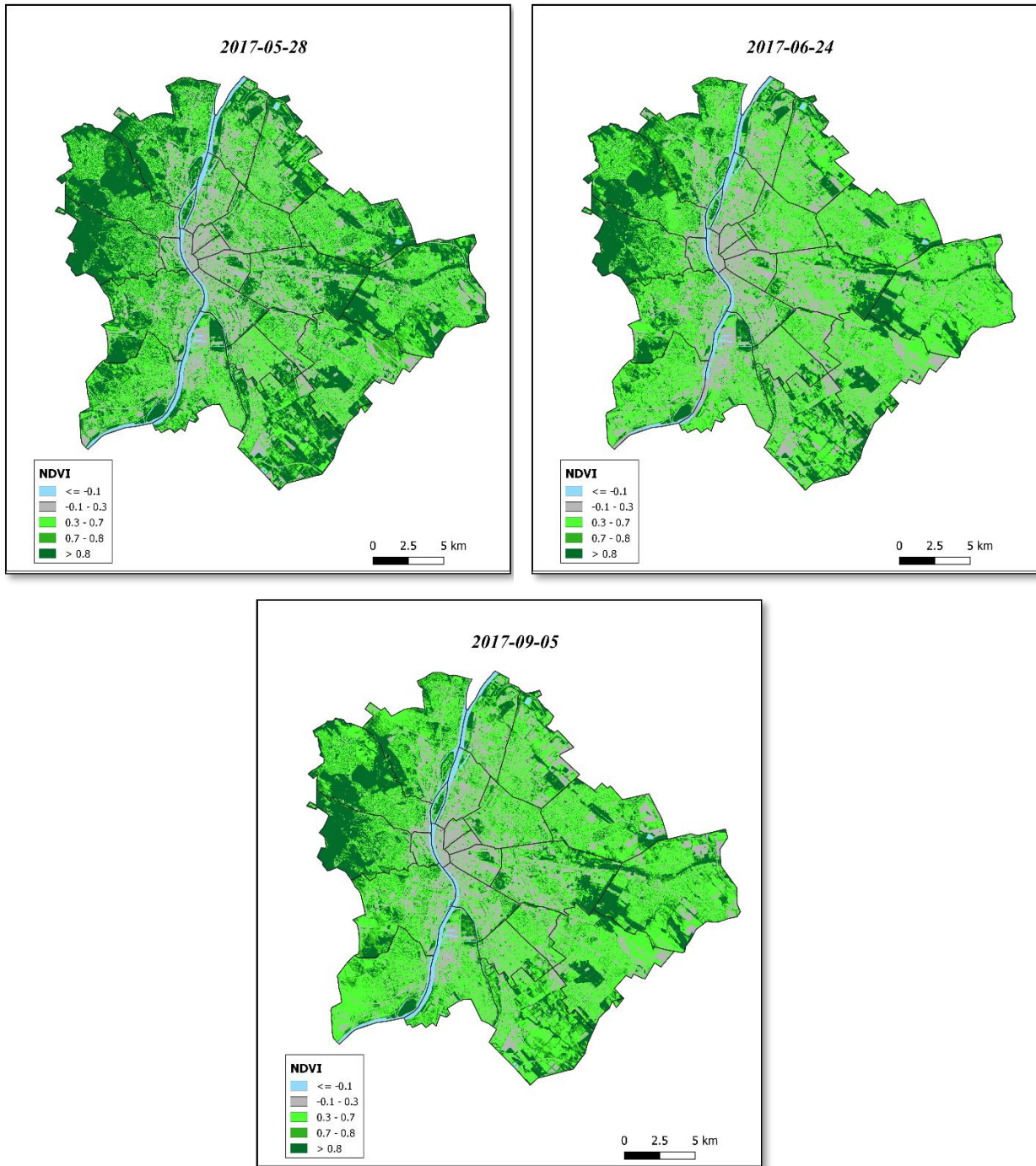


Fig. A 1. NDVI images for Budapest (1/5).

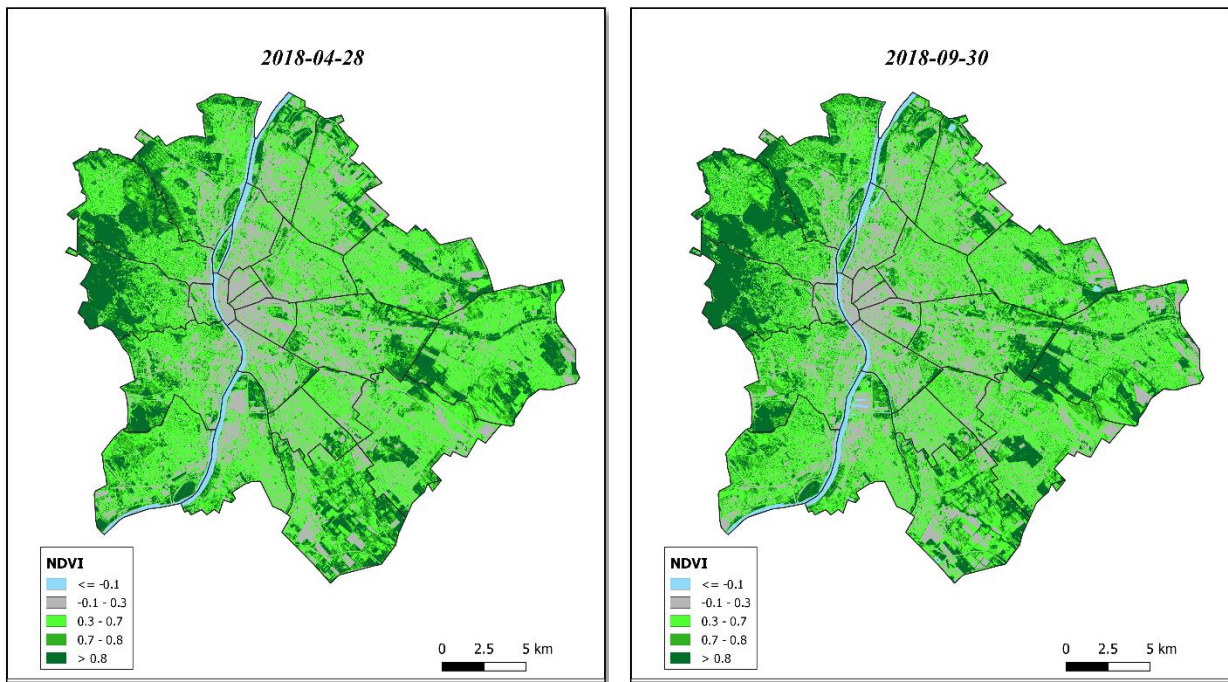


Fig. A 2. NDVI images for Budapest (2/5).

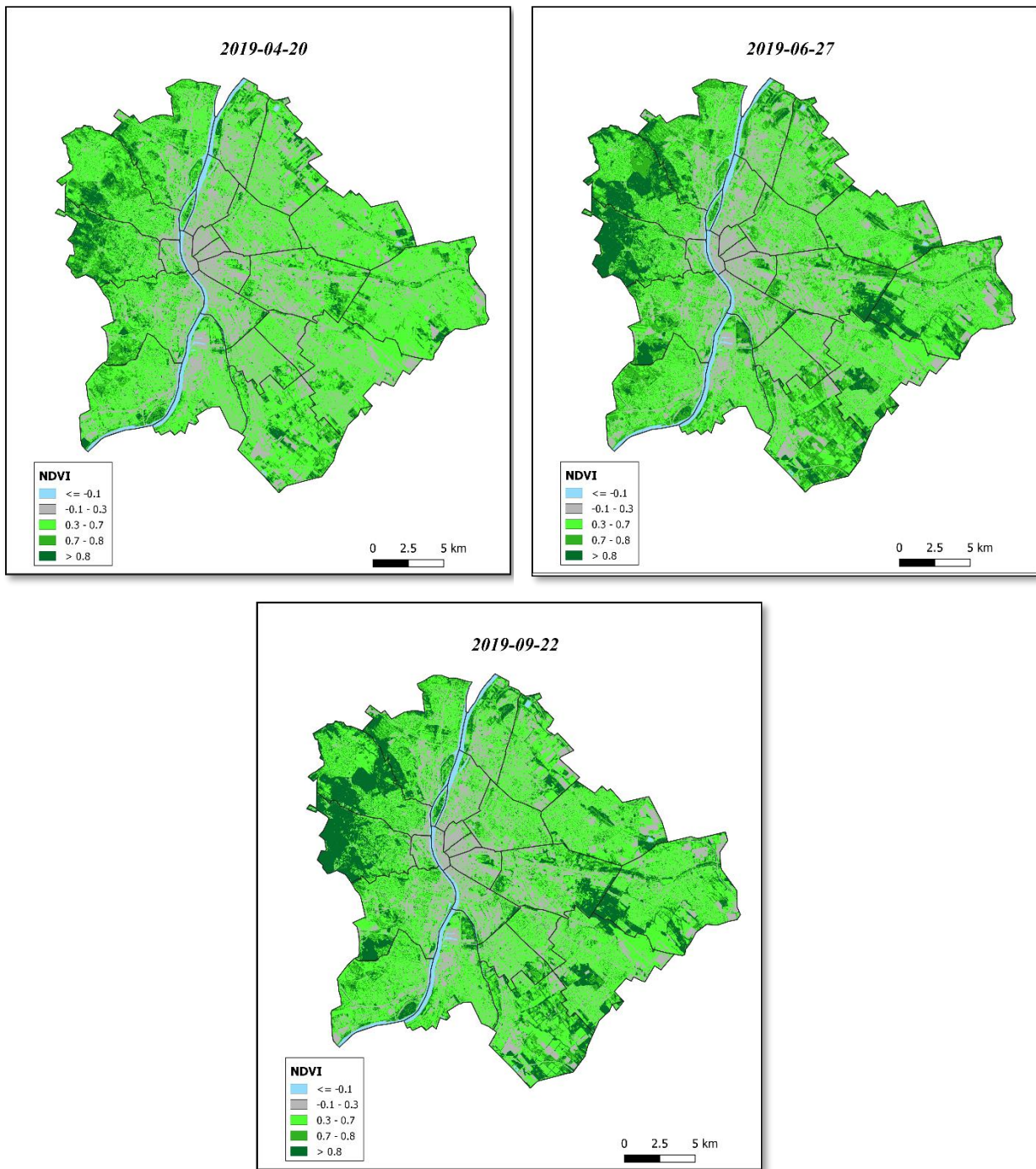


Fig. A 3. NDVI images for Budapest (3/5).

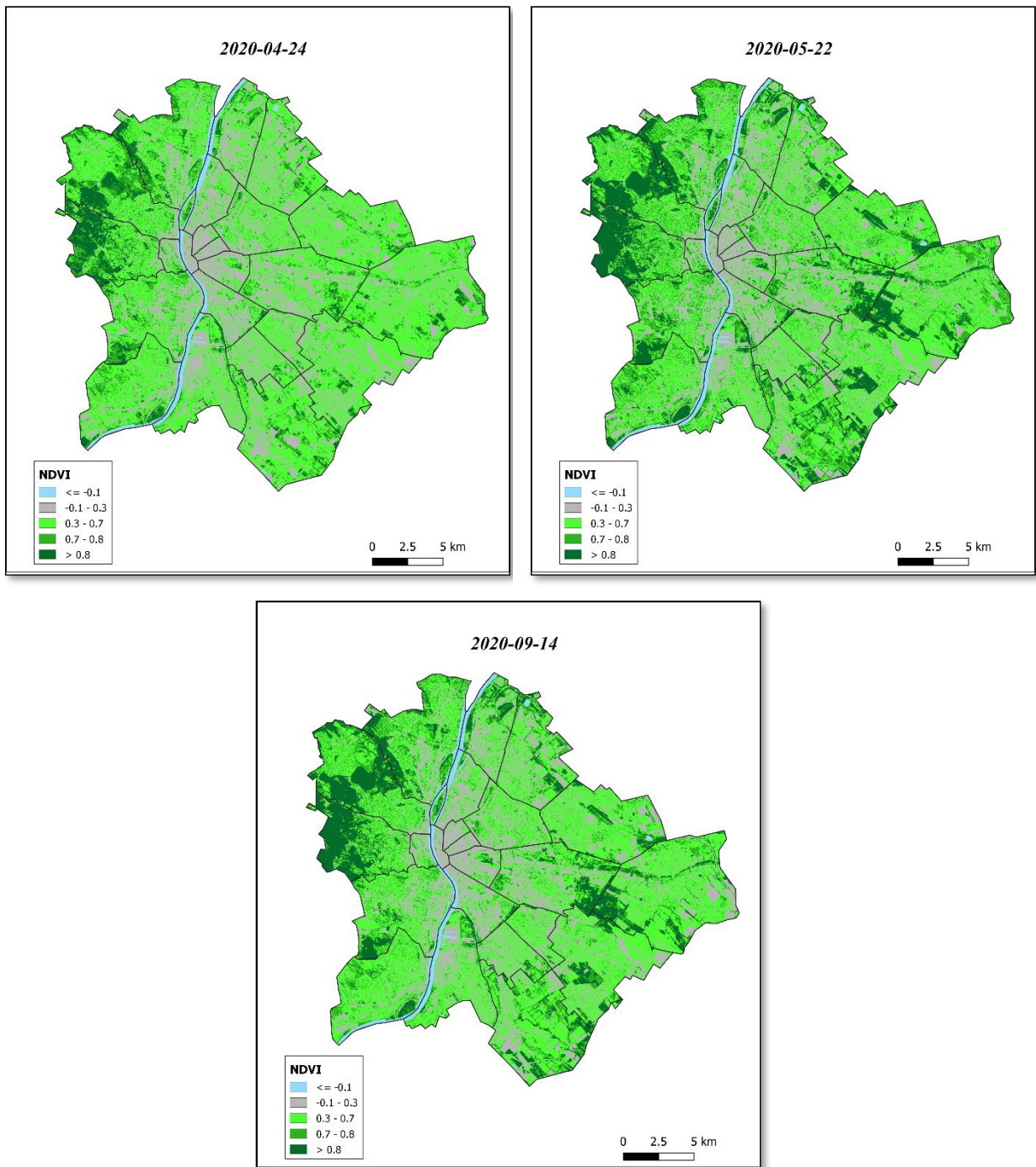


Fig. A 4. NDVI images for Budapest (4/5).

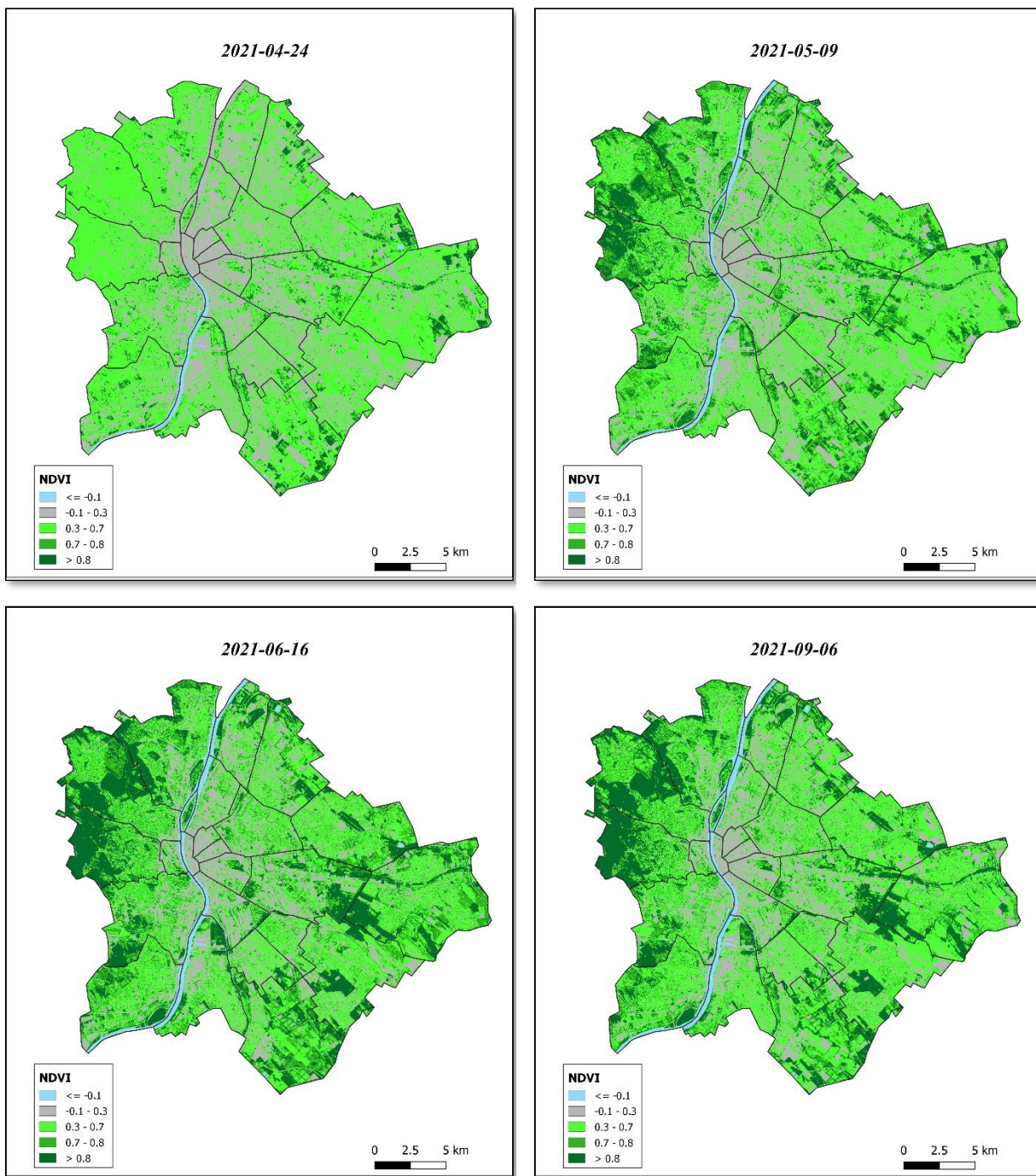


Fig. A 5. NDVI images for Budapest (5/5).

Classification

2017

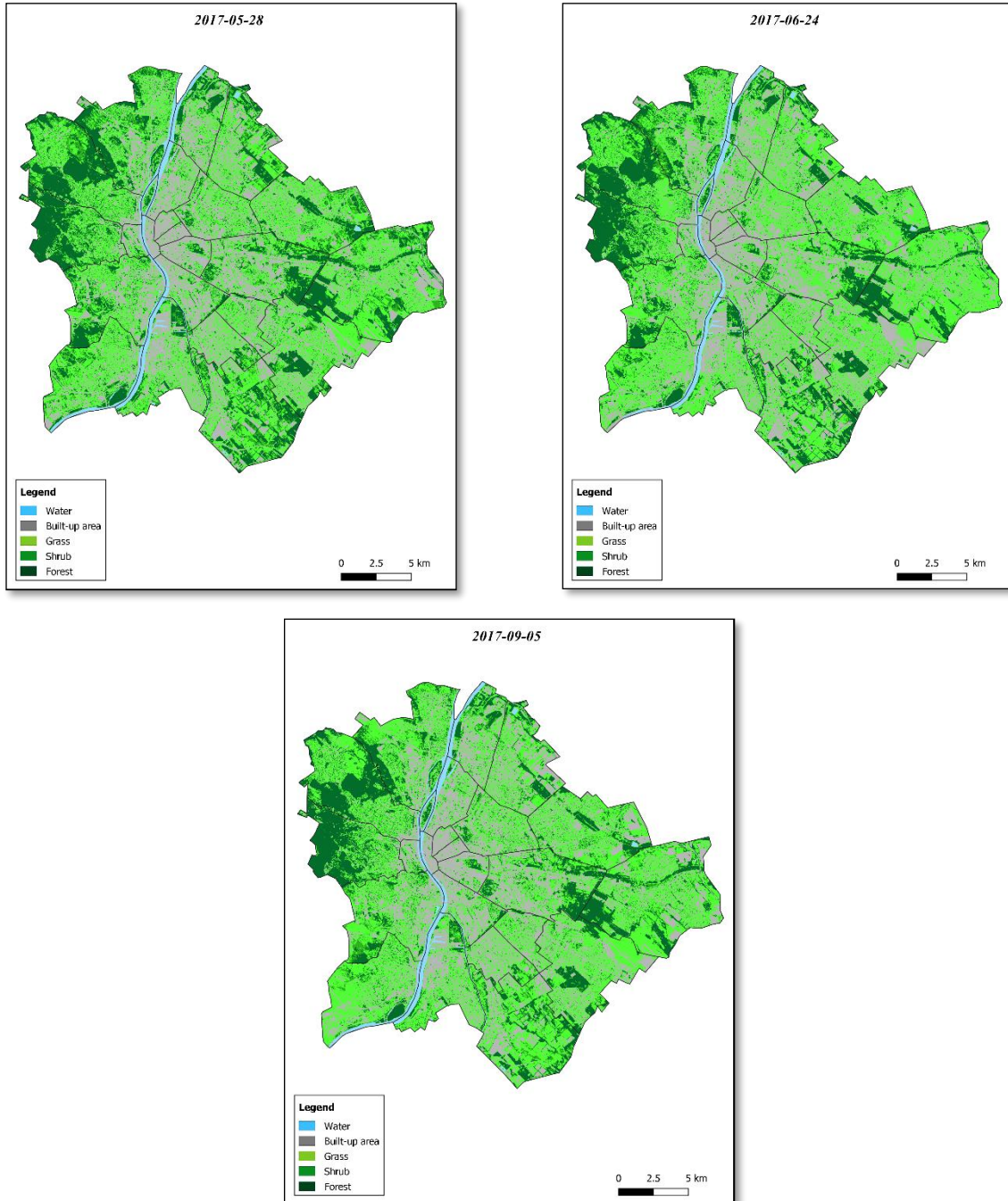


Fig. A 6. Classified images based on NDVI images for Budapest (1/5).

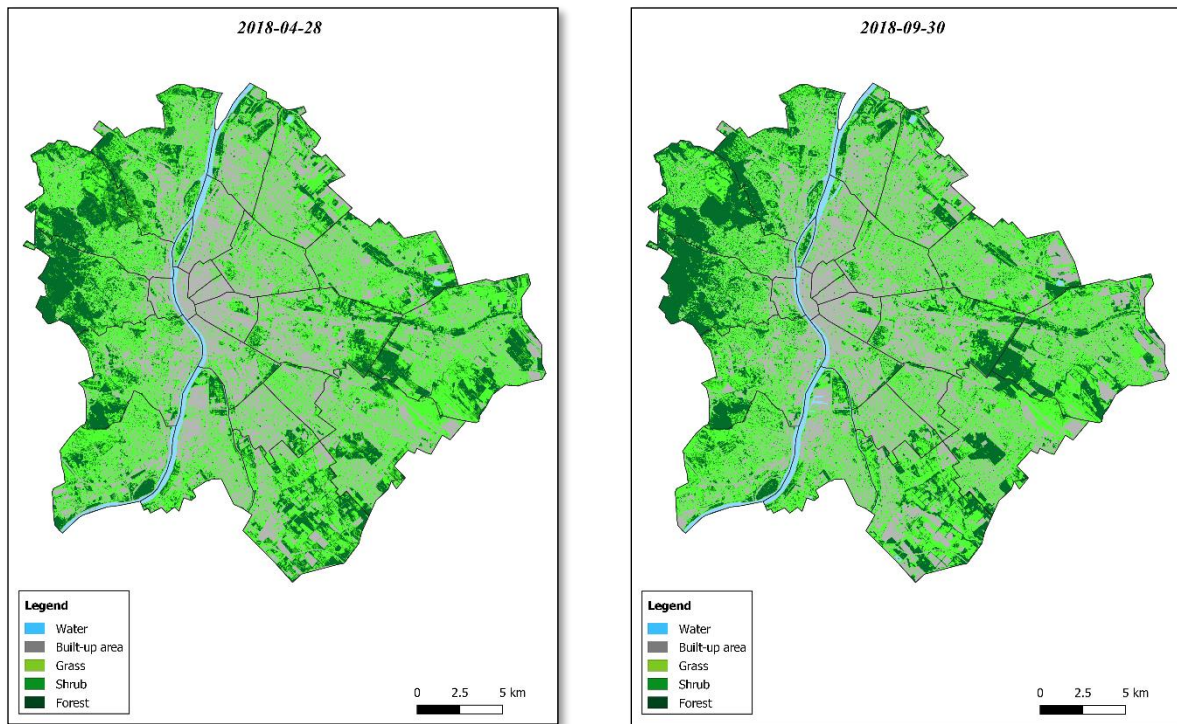


Fig. A 7. Classified images based on NDVI images for Budapest (2/5).

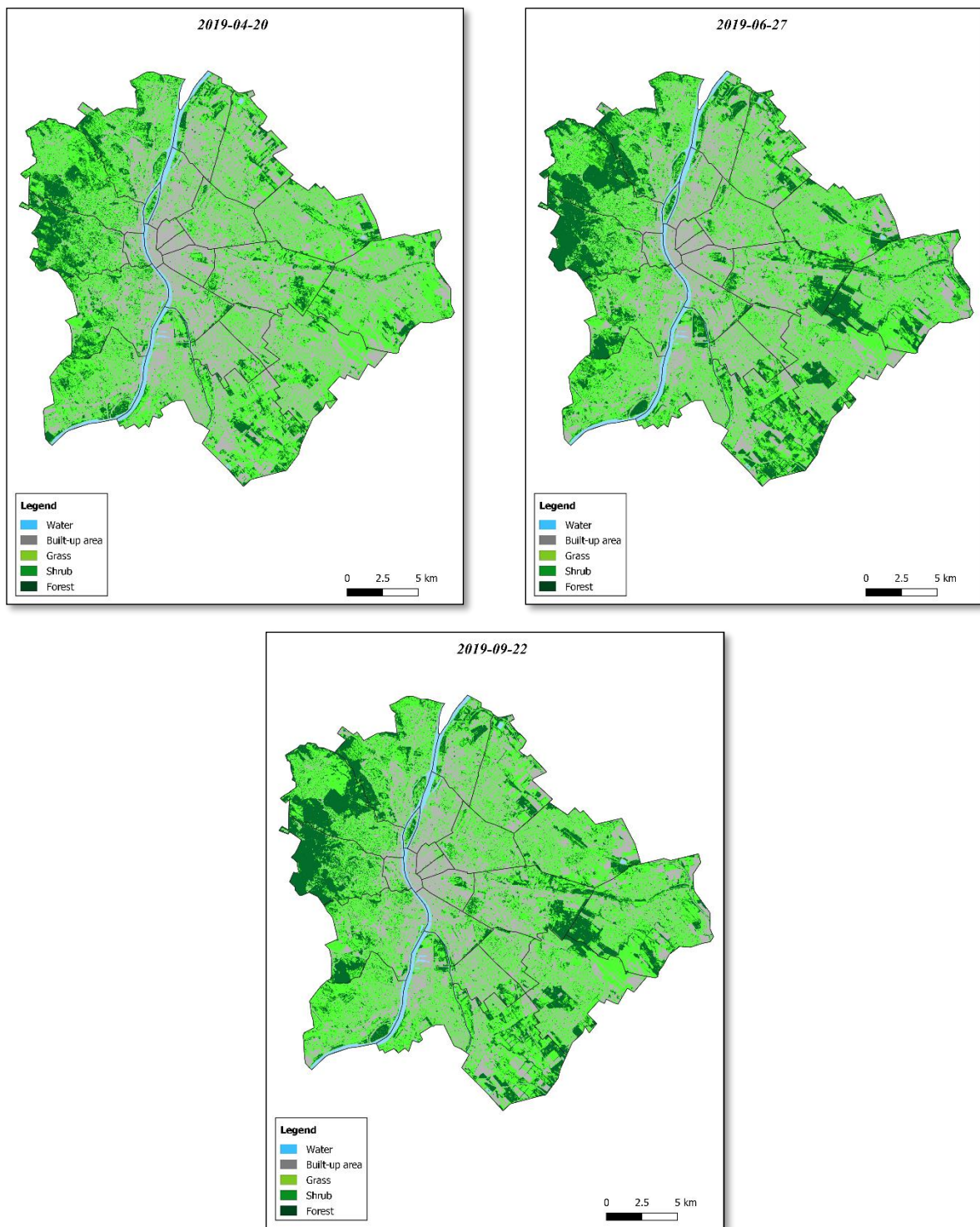


Fig. A 8. Classified images based on NDVI images for Budapest (3/5).

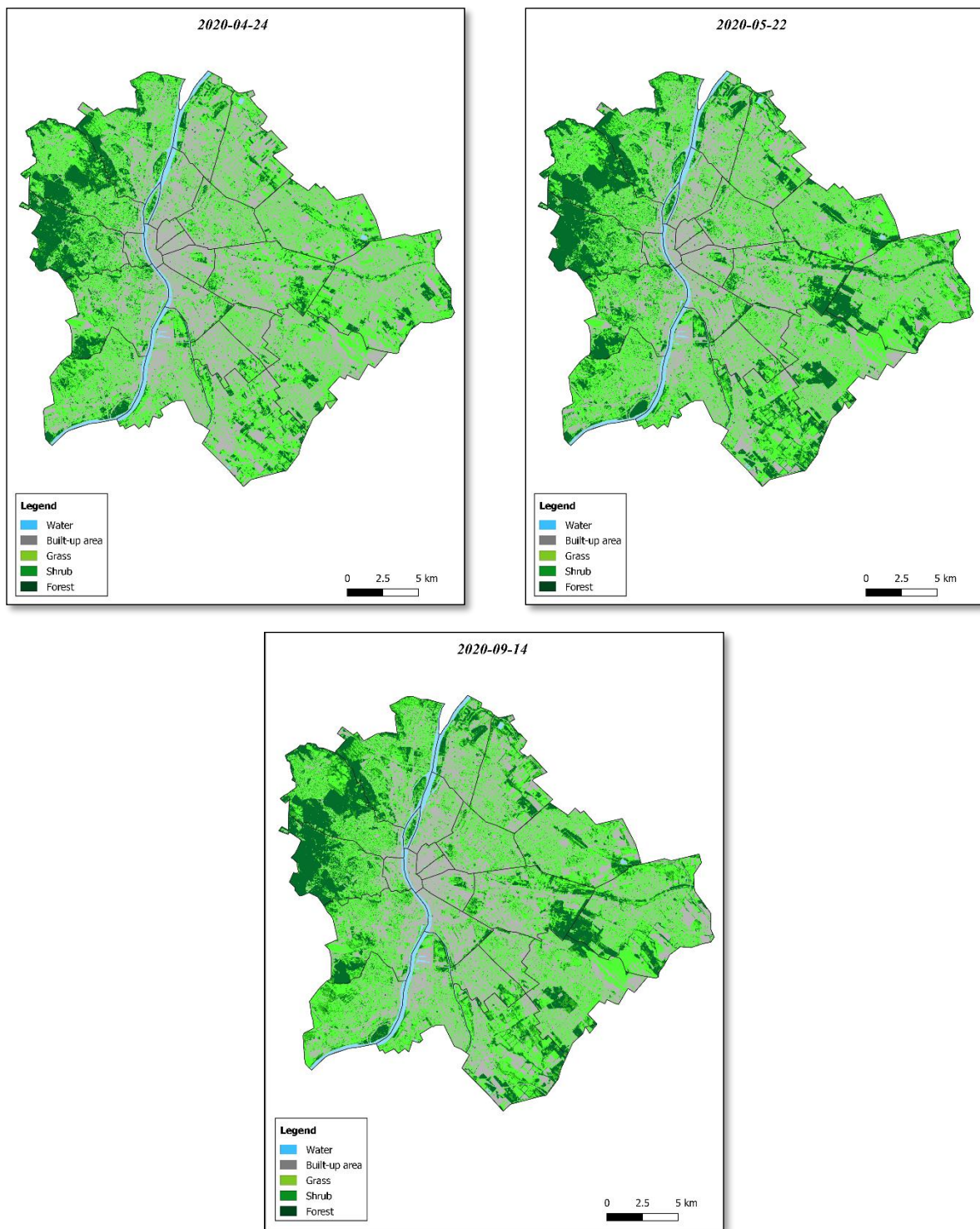


Fig. A 9. Classified images based on NDVI images for Budapest (4/5).

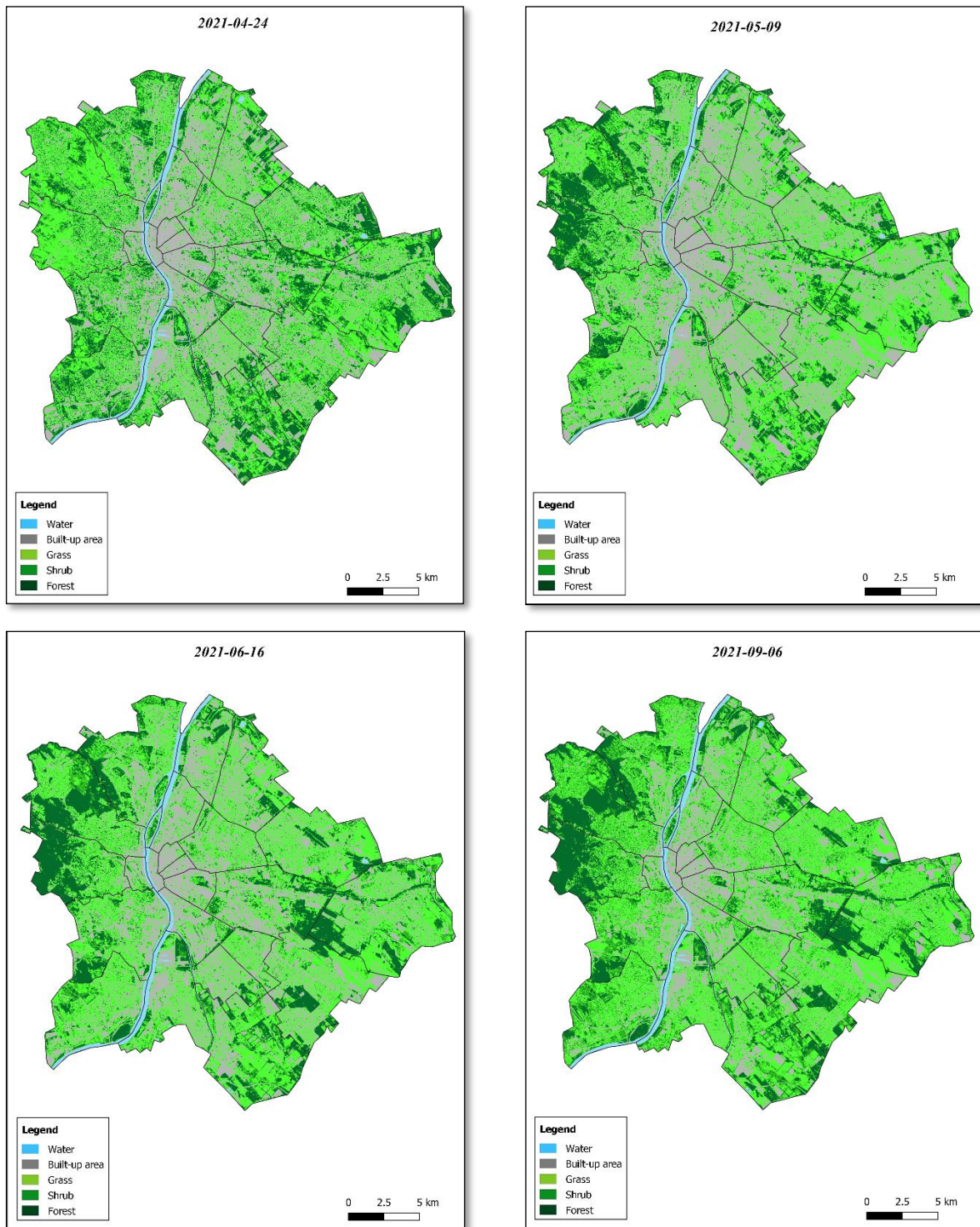


Fig. A 10. Classified images based on NDVI images for Budapest (5/5).

DECLARATION

I, undersigned *Ali Dowajy* (NEPTUN CODE: *LL8L65*), declare that the present master's thesis is my original intellectual product in full and that I have not submitted any part or the whole of this work to any other institution. Permissions related to the use of copyrighted sources in this work are attached.

I AGREE to the publication of the accepted master's thesis in pdf form on the website of the Institute of Cartography and Geoinformatics.

Budapest, *15, May, 2022*



(signature of the student)